FAA-RD-77-31

Project Report
ATC-74

Coaxial Magnetron Spectra and Instabilities

M. Labitt

24 June 1977

Lincoln Laboratory
MASSACHUSETTS INSTITUTE OF TECHNOLOGY
LEXINGTON, MASSACHUSETTS

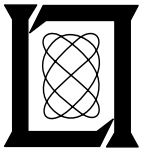

Prepared for the Federal Aviation Administration,
Washington, D.C. 20591

This document is available to the public through
the National Technical Information Service,
Springfield, VA 22161

1. Report No.	2. Government Accession No.	3. Recipient's Catalog No.
FAA-RD-77-31		

4. Title and Subtitle	5. Report Date
Coaxial Magnetron Spectra and Instabilities	24 June 1977
	6. Performing Organization Code

7. Author(s)	8. Performing Organization Report No.
M. Labitt	ATC-74

9. Performing Organization Name and Address	10. Work Unit No. (TRAIS)
M.I.T. Lincoln Laboratory P.O. Box 73 Lexington, MA 02173	11. Contract or Grant No. Task K DOT-FA71-WAI-242
	13. Type of Report and Period Covered
12. Sponsoring Agency Name and Address Department of Transportation Federal Aviation Administration Systems Research and Development Service Washington, DC 20591	Project Report
	14. Sponsoring Agency Code

15. Supplementary Notes

This work was performed at Lincoln Laboratory, a center for research operated by Massachusetts Institute of Technology under Air Force Contract F19628-76-C-0002.

16. Abstract

Application of advanced radar clutter rejection techniques to FAA airport surveillance and enroute radars is constrained by inherent instabilities and spectral properties of the device used in the radar transmitter to generate high level RF pulse energy, and the degree to which its spectrum can be influenced by the circuit in which it operates. Coaxial magnetrons are believed to be spectrally pure, controllable and stable, and to embody other characteristics such as long life, which make them attractive replacements for the magnetrons presently employed. This report summarizes the results of extensive measurements made on a conventional S-band magnetron (presently employed in the ASR-7 radar) and a coaxial magnetron of equivalent pulse and power rating to compare their instabilities and spectral properties.

17. Key Words	18. Distribution Statement
Coaxial Magnetron Stability Spurious Response Airport Surveillance Radars Moving Target Indicator	Document is available to the public through the National Technical Information Service, Springfield, VA 22151

19. Security Classif. (of this report)	20. Security Classif. (of this page)	21. No. of Pages	
Unclassified	Unclassified	74	

TABLE OF CONTENTS

ILLUSTRATIONS

ILLUSTRATIONS (continued)

COAXIAL MAGNETRON SPECTRA AND INSTABILITIES

I. INTRODUCTION

This report covers measurements and analyses performed by Lincoln Laboratory for the Federal Aviation Administration in order to compare the emissions of a coaxial and a conventional magnetron operating in the frequency range of 2700 to 2900 MHz. The study was authorized under Task K of Interagency Agreement DOT-FA71-WAI-242.

The coaxial magnetron investigated in this study was the Raytheon QK1739LL. It was developed as a replacement tube for the magnetron presently used in the ASR-7 airport surveillance radar. The conventional magnetron studied was the Amperex DX276* normally used in the ASR-7.

Magnetron characteristics measured and used as the basis of comparison were:

- short term stability (frequency jitter)
- long term stability (thermal drift)
- spurious response (18 GHz to waveguide cutoff)
- pulse characteristics (applied voltage and current waveforms and time jitter)
- pulling and pushing figures
- compliance with OTP "Radar Spectrum Engineering Criteria", Part 5.

Subtasks necessary to accomplish Task K were:

1. Develop, build and operate circuitry to
   a. control the rate of rise of the voltage applied to the coaxial magnetron.
   b. inject a priming signal into the coaxial magnetron.
   c. measure frequency jitter.
2. Determine the ability of the coaxial magnetron to lock to a low-level priming signal.

---

*Equivalent to the Raytheon 5586 tube.

3. Ascertain the effect of the coaxial magnetron's priming signal on rise-time jitter.

4. Seek techniques to improve the conventional magnetron spectrum by the use of the special circuits developed to control the rate of rise of applied voltage.

II. MAGNETRON OPERATION

A. Coaxial Magnetron

To perform the coaxial magnetron measurements an ASR-7 radar transmitter and receiver were obtained. Modifications to the ASR-7 modulator were necessary since the coaxial magnetron requires that the modulator generate a much slower voltage pulse rise-time than the DX276 normally requires. If the rate of rise is too fast (>65K volts per μsec), the coaxial tube will tend to mode causing the generation of off-frequency energy, severe modulator mismatch and RF rise-time jitter. A sudden threshold of moding does not appear to exist, however the probability of moding rapidly increases with the rate of rise.

It was found that the present method of increasing rise time, i.e. adding inductance in series with the pulse forming network (PFN), was inadequate. This method did slow the rise time, but it also increased the fall time to such an extent that the RF envelope was severely distorted (Figure 1), and the spectrum degraded. Also, the additional inductance mismatched the modulator and essentially transformed the PFN into a one-section network.

In order to increase rise-time and not affect fall-time, a special non-linear diode network was developed. Its circuit is shown and its method of increasing rise-time without affecting fall-time is explained in Figure 2. A typical spectrum using the diode network is shown in Figure 4. A coax magnetron spectrum taken using the series inductance is shown in Figure 5.

B. Conventional Magnetron

Initially it was believed that the diode network concept would be useful in controlling the spectrum of the DX276. In the normal configuration a two-section PFN is used together with an RC despiking network. This results in a long RF

ATC-74(1)

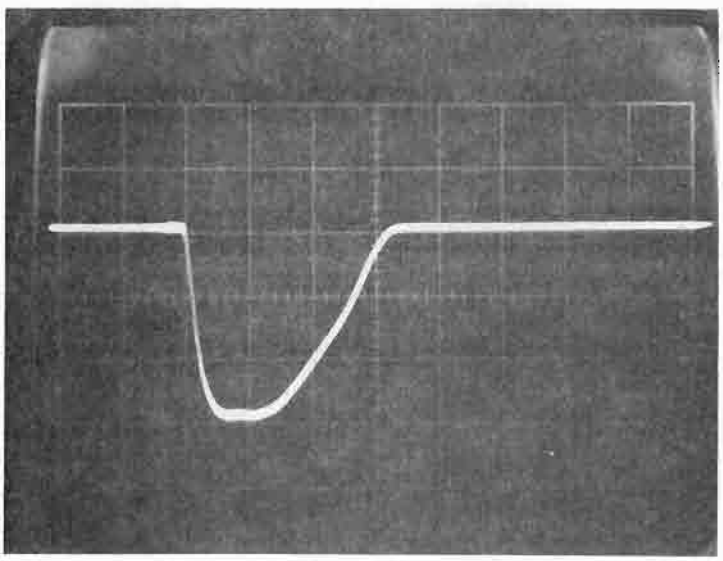

Fig. 1. RF pulse excessive fall-time caused by inductive control of rise time.

Operation of Diode Network of Fig. 2: After the first pulse, the 250 pf capacitor charges to the magnetron pulse voltage and then decays to a value below the conduction voltage of the magnetron. This voltage is set by the Zener diode stack. On the second and subsequent pulses, the fast recovery diodes are normally biased off. When the magnetron pulse is applied the capacitor loads the pulse transformer increasing the rise time after the pulse voltage exceeds the Zener stack voltage. This loading only lasts approximately as long as the time constant RC = 250 nsec, where R = 1000 ohms is the source impedance of the modulator.

The result is that the magnetron voltage rises rapidly at first, (as shown by the more distinct trace in Fig. 3a), then abruptly slows down just before the magnetron starts to conduct and oscillate. (The RF envelope is shown as the more distinct trace in Fig. 3b). Notice that when the modulator pulse shuts off, the charge on the capacitor does not discharge through the magnetron to produce a long RF pulse tail, but instead discharges harmlessly through the Zener stack.

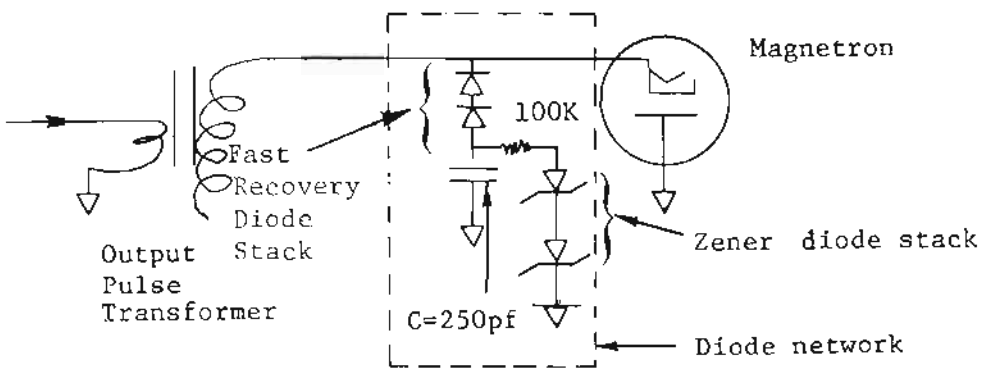

Fig. 2. Diode network used to control magnetron voltage rate of rise.

ATC-74(3a)

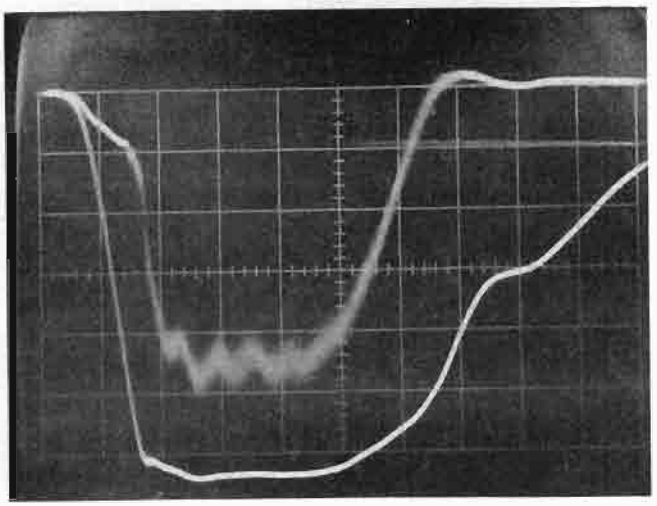

Fig. 3a. V-I waveforms - coaxial magnetron (upper curve is I) (H-axis: 0.2 μsec/div; V-axis: 10 amps/div and 5 KV/div).

ATC-74(3b)

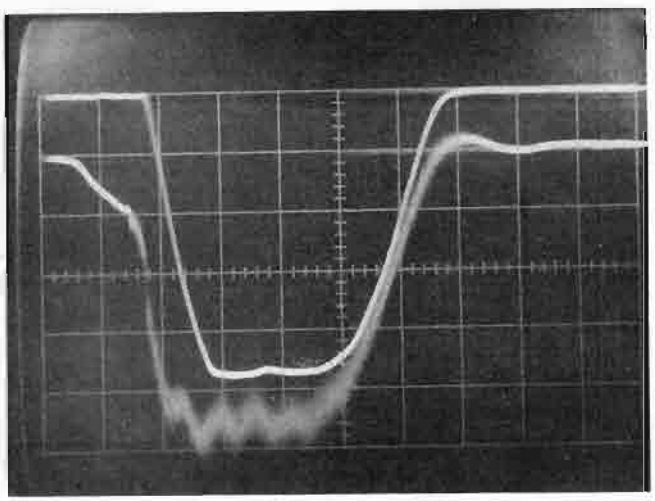

Fig. 3b. I-P_{out} waveforms - coaxial magnetron (upper curve is linear P_o, not calibrated).

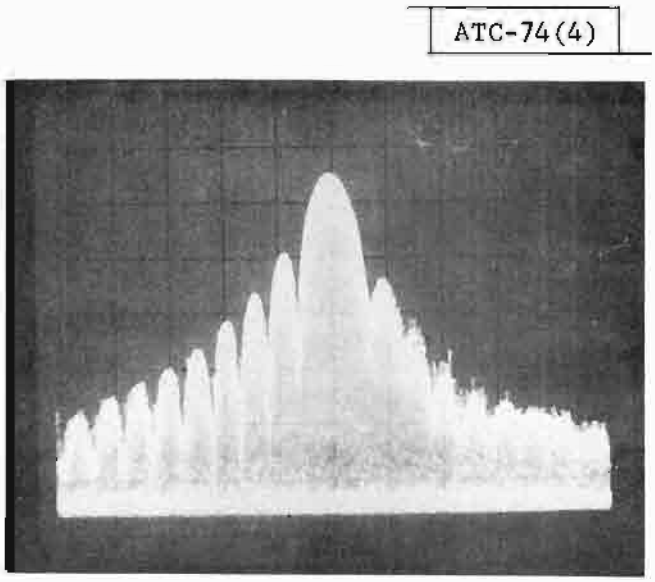

Fig. 4. Typical coaxial magnetron spectrum (V-axis: 10 dB/div; H-axis: 2 MHz/div).

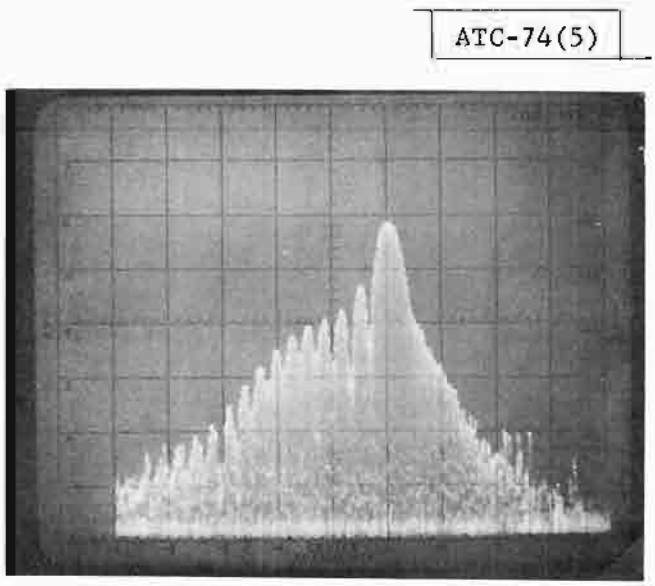

Fig. 5. Coaxial magnetron spectrum using inductor in series with PFN (V-axis: 10 dB/div; H-axis: 2 MHz/div).

tail which causes the high side lobes on the low frequency side of the spectrum. To control the long tail the old PFN was replaced with a 10-section network. This network reduced the fall-time but also reduced the rise-time. The diode network was then used to control the fast rise time (as with the coax magnetron) in order to prevent the tube from moding.

Figure 6 shows the spectrum using the 10-section network and the diode network. Figure 7 shows the standard configuration spectrum. An improvement is apparent but it is not deemed worth the additional complexity. DX276 measurements described in the rest of this report are all made using the standard configuration of the ASR-7 radar transmitter/modulator.

III. MEASUREMENT RESULTS

A. Short-Term Frequency Stability

1. Importance of Short-term Frequency Stability

Modern MTI radar processors require that the transmitter have a high degree of frequency stability. The effect of frequency fluctuation can be demonstrated by the following situation. Consider the radar return from two ranges separated by a half a pulse length at the same azimuth. Upon arrival at the radar the two returns will partially overlap. If the radar frequency varies from pulse to pulse, then the resultant signal level at the overlap point will fluctuate. Most modern MTI devices process the signal after the steady component has been removed. Thus, in a conventional MTI radar frequency instability will increase the number of false alarms, while in a CFAR MTI the frequency instability will result in a loss of sensitivity.

Consider a perfectly stable radar (other than the magnetron frequency) looking at stationary clutter and define the ratio of the fluctuation to steady components as ϕ, T the pulse length; then the relationship to the frequency filter is:

$$f_{rms} = \frac{\sqrt{3\phi}}{\pi T} \qquad (1)^*$$

*Equations (1) and (2) are derived in the Appendix.

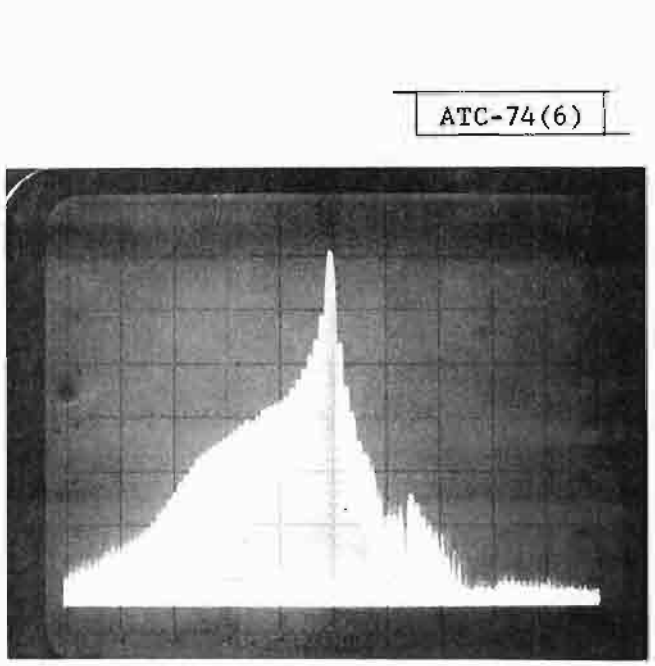

Fig. 6. DX-276 spectrum using diode network and 10-section PFN (V-axis: 10 dB/div; H-axis: 10 MHz/div).

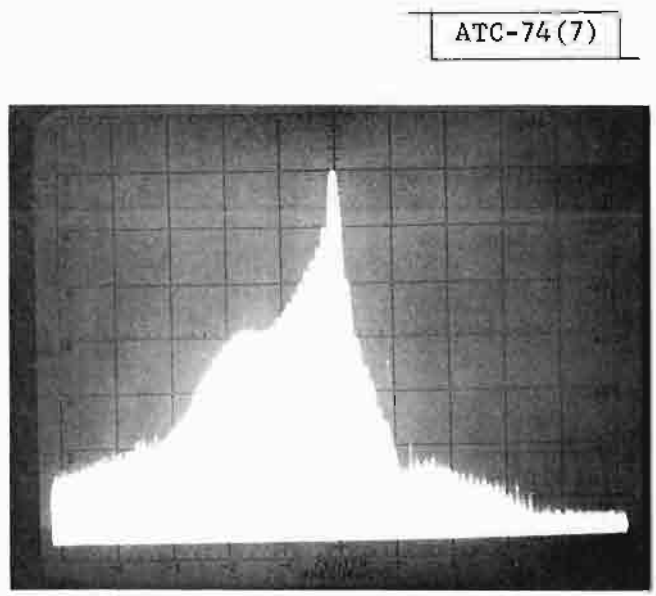

Fig. 7. DX-276 spectrum using standard configuration (V-axis: 10 dB/div; H-axis: 10 MHz/div.

if the coho is locked to the center of the magnetron pulse. If the coho is locked to the tail of the pulse, then the requirement is more stringent,

$$f_{rms} = \frac{\sqrt{3\phi}}{2\pi T} \qquad (2)^*$$

Normally the coho is locked to the tail, but it does not prove to be much of a problem to do mid-pulse locking. If a residue-to-clutter ratio of 0.16×10^{-4} (-48 dB) and a pulse length of 0.7 μsec are assumed, then for a center-locking system, the magnetron jitter should not exceed

$$f_{rms} = 3150 \text{ Hz} \qquad (3)$$

A ϕ of -48 dB represents a loss in the processor improvement factor of 0.64 dB when operating at a clutter-to-thermal-noise ratio of 40 dB.

2. Measurement Technique

A short-term frequency stability measurement setup is shown in Figure 8. An attenuated sample of the RF pulse is mixed down to 30 MHz and then split into two paths; one delayed and the other not. The delay consists of a length of cable and is 0.35 μsec long corresponding to about half the magnetron pulse length. The effect is to beat the first half of the pulse with the back half. The response of a phase detector is

$$E = kAB \sin \theta$$

where E is the output voltage, A and B are the amplitudes of the two signals, k is a constant and θ the phase difference. Notice that E can only be greater than zero when both A and B are greater than zero. Consequently, the phase detector output will appear on a scope as in Figure 9a in an idealized form. A sample and hold (S/H) is set to sample the phase detector in the center of the overlap. The line stretcher is adjusted so that θ is near zero and, as a result, the output of the sample and hold is proportional to the phase difference, θ, as long as θ is small.

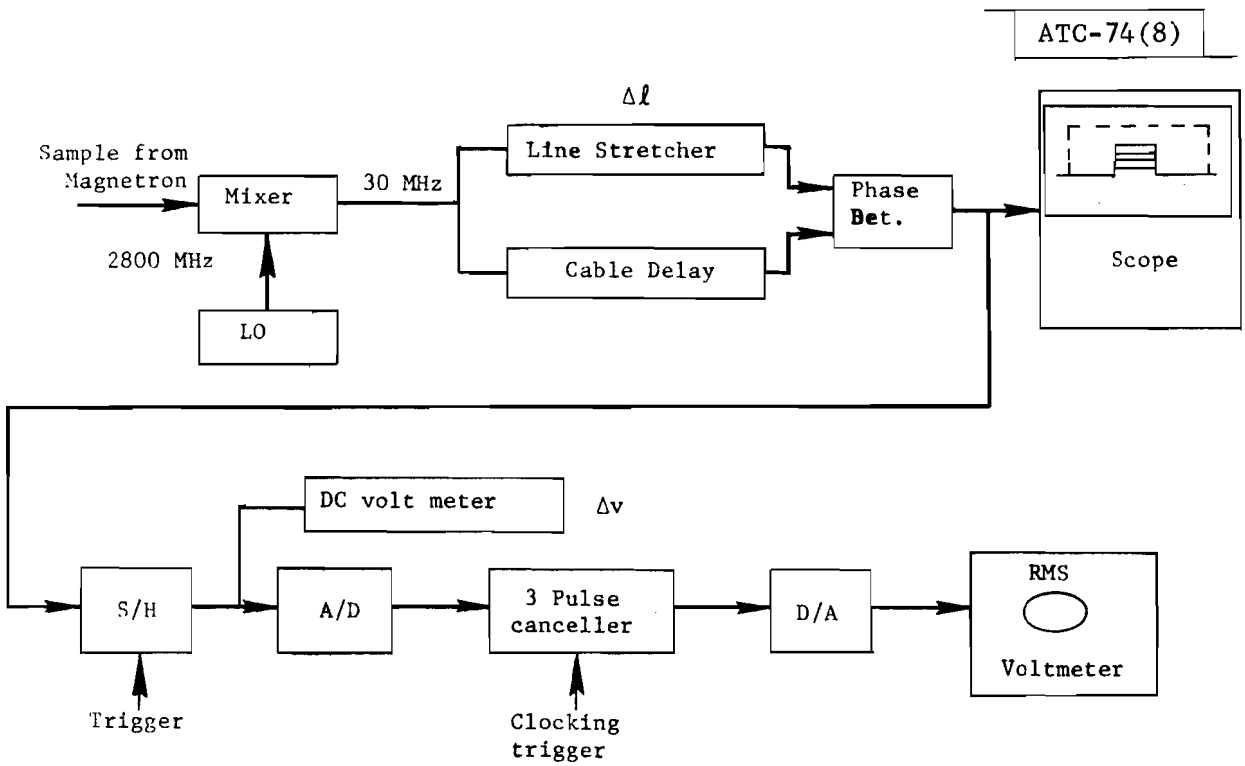

Fig. 8. Short term frequency stability test set-up.

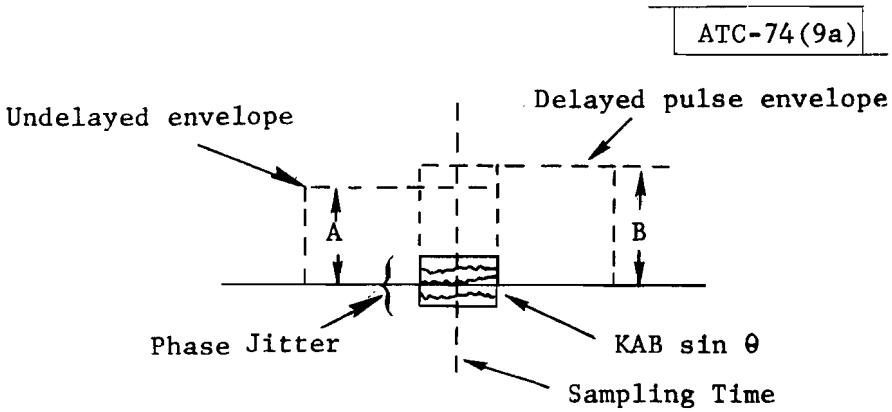

Fig. 9a. Phase detector operation.

The relationship between the magnetron jitter, f_{rms}, and θ can be determined by tracing the signal through the various components (Figure 8). The FM jitter at RF is converted down to the same amount of jitter at the 30-MHz IF. The phase at the phase detector is therefore,

$$\theta = 2\pi f_{IF} T$$

where f_{IF} is the FM'd IF frequency, and T is the cable delay time. A change in θ is given by

$$\delta\theta = 2\pi T \delta f_{IF}$$

or

$$\theta_{rms} = 2\pi T f_{rms}$$

where f_{rms} is the standard deviation of the magnetron frequency and defined as

$$f_{rms} \triangleq \left[E\{(f_{mag} - E\{f_{mag}\})^2\}\right]^{1/2}$$

where $E\{\ \}$ is the expectation (averaging) operator. Notice that f_{rms} is not really the rms value of the frequency, but the rms value of the difference from the mean. However, this definition is common and will be used here.

In order to measure θ_{rms} it is necessary to first remove the DC component. This is accomplished by converting the signal out of the "sample and hold" (S/H) to digical and then through a 3-pulse canceller (as in an MTI system). The signal is then converted back to analog and finally fed to an rms voltmeter. In addition to removing the DC component, the 3-pulse canceller removes the effect of any slow drift of phase (or frequency). Such drift would not affect an MTI system.

The 3-pulse canceller has the following response,

$$R_n = E_n - 2 E_{n-1} + E_{n-2}$$

where E_n is the nth voltage sample. Thus, the rms voltmeter measures this quantity,

$$R_{rms} = \left[E \{ (E_n - 2 E_{n-1} + E_{n-2})^2 \} \right]^{1/2}$$

Because E_n and E_m are not correlated.

$$E \{E_n E_m\} = \bar{E}_n \bar{E}_m = \bar{E}^2$$

where the bar denotes the average. Thus,

$$\begin{aligned} R_{rms} = \Big[& E \{ E_n^2 - 2 E_n E_{n-1} + E_n E_{n-2} \\ & -2 E_n E_{n-1} + 4 E_{n-1}^2 - 2 E_{n-1} E_{n-2} \\ & + E_n E_{n-2} - 2 E_{n-1} E_{n-2} + E_{n-2}^2 \} \Big]^{1/2} \\ = & \left[6 E \{ E_n^2 \} - 6 \bar{E}^2 \right]^{1/2} \end{aligned}$$

or

$$R_{rms} = \sqrt{6}\ E_{rms}$$

Calibration is necessary and is performed in the following manner. The line stretcher, on the LO, is first adjusted so the DC voltmeter (Figure 8) indicates zero. Then the line stretcher is moved a known distance, $\Delta \ell$, and the corresponding change in DC voltage ΔV noted. The phase shift per volt is then,

$$\frac{\Delta \theta}{\Delta V} = \frac{2\pi\ \Delta \ell}{\Delta V\ \lambda_{IF}} = \frac{2\pi\ \Delta \ell\ \ f_{IF}}{C\ \ \Delta V}$$

where λ_{IF} is the IF wavelength and C is the velocity of light. Remembering that

$$f_{rms} = \frac{\theta_{rms}}{2\pi\ T}$$

and

$$\theta_{rms} = \frac{R_{rms}}{\sqrt{6}} \quad \frac{\Delta \theta}{\Delta V}$$

we can condense all of the above to

$$f_{rms} = \frac{R_{rms}\, f_{IF}}{\sqrt{6}\ CT} \quad \frac{\Delta \ell}{\Delta V}$$

3. Coaxial Magnetron

It was determined that heater power, and to a lesser extent operating frequency, affects the short-term frequency stability of the coaxial magnetron. All other parameters appear to have a minor effect. Figure 9b shows the standard deviation of frequency (f_{rms}) as a function of both heater voltage and output frequency. The nominal heater voltage for any magnetron depends on the particular value of average anode power applied and, for this situation, is about 58 volts. The standby voltage is 70 volts. It can be seen that stability markedly improves as the heater voltage is raised to presumably an excessive value. Both Raytheon and Lincoln believe that this phenomenum is peculiar and does not represent the capability of the coaxial magnetron. Raytheon believes it to be a cathode phenomenum (perhaps caused by the leakage of cathode material over the end caps) and that the effect can be eliminated by a different cathode design. Such different cathode designs have been used in the production of higher frequency coaxial magnetrons. As it stands now, the only way to have this magnetron meet the requirements of Eq. (3) is to raise the heater voltage to 70 volts. Raytheon believes this will not shorten tube life.

4. Conventional Magnetron

Measurements of the Amperex DX276 have been made at 2.7, 2.8 and 2.9 GHz. No statistically significant differences were noted. Unlike the coaxial tube, the DX276 is not heater power sensitive. The standard deviation of frequency was measured several times at each frequency and found to be

$$f = 2068 \pm 660 \text{ Hz}$$

B. Long-Term Frequency Stability

Measurements have been taken on both magnetrons of the shift in frequency and the rise in temperature that occurs when the tubes are first turned on. Such information is useful in determining how much frequency bandwidth is occupied during warmup.

ATC-74(9b)

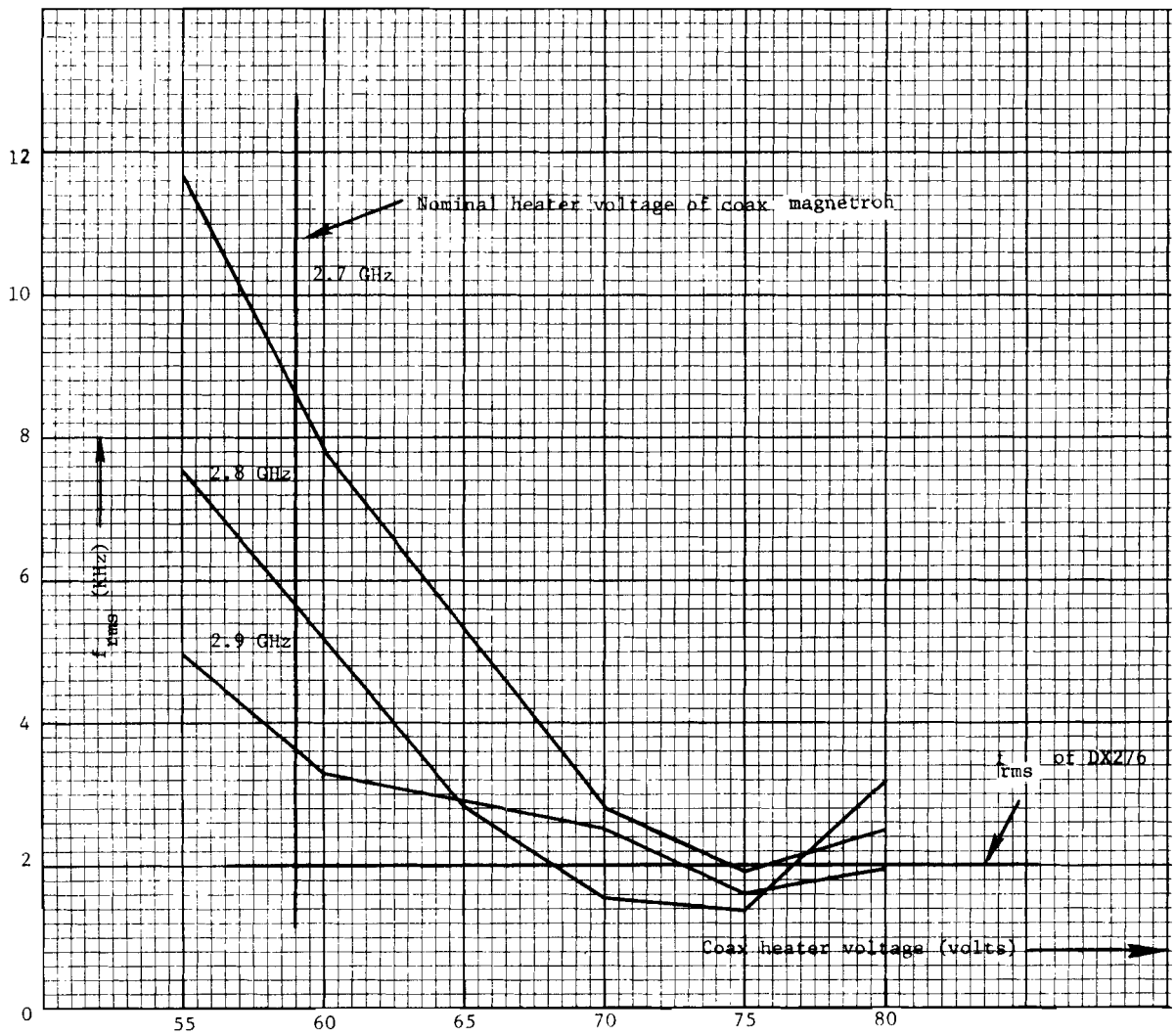

Fig. 9b. f_{rms} of coaxial magnetron vs frequency.

The frequency drift was measured by observing the spectrum drift across the screen of a spectrum analyzer. Because the anode portion of the tube was inaccessible, the temperature of the coaxial tube was measured by recording the temperature of air coolant exhausting from the tube. The temperature of the 5586 was measured using thermo-couples directly attached to the tube anode.

1. Coaxial Magnetron

The frequency temperature shift of the QK1739 is plotted in Figure 10 for three trials. The maximum frequency drift is about 1.5 MHz and takes about an hour to occur. No frequency change occurred until about 3-4 minutes had elapsed even though the exhaust temperature has started to rise. The exhaust temperature levels out to about $48^{o}C$.

2. Conventional Magnetron

Figure 11 illustrates how the DX276 drifts during warmup. Note that half of the total frequency excursion of 7 MHz occurs in 8 minutes. In contrast, the coaxial tube takes about 18 minutes to drift to half its total excursion. The frequency drift rate is greatest at turnon. The anode temperature reads $90^{o}C$, half of which occurs in the first four minutes.

C. Spurious Responses

1. Measurement Technique

Spectral measurements using the Hewlett-Packard 141T spectrum analyzer (8555A RF section, 8552B IF section and 8445B tracking preselector) have been made of the two magnetrons operating at 2.7, 2.8 and 2.9 GHz. The dynamic range (linear) of the H-P analyzer is limited to about 60 dB. Consequently, in order to extend the range to the required 100 dB, a notch filter was employed to suppress most of the main lobe energy. This allowed the signal strength (sensitivity) outside the main lobe area to be increased so that any spurious responses 100 dB down from the main lobe would be observable. At frequencies above the main lobe the notch filter passband is not flat and therefore is ineffective. Here C, X and K-band waveguides were used to remove the main lobe. The signal from the probe went through a coax to waveguide

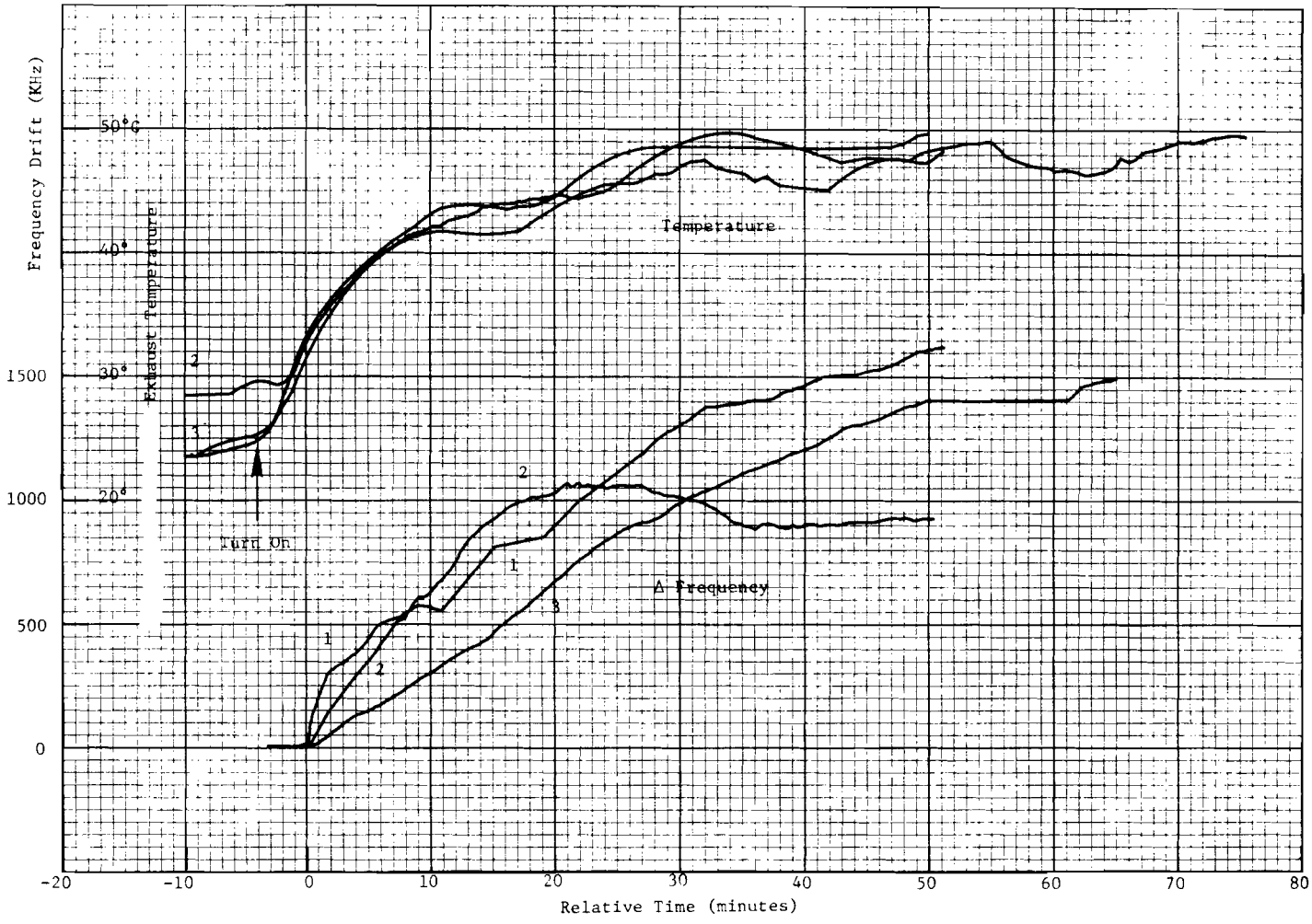

Fig. 10. Frequency drift and exhaust temperature rise of coaxial magnetron (QKH-1739LL); ASR-7 normal operating conditions.

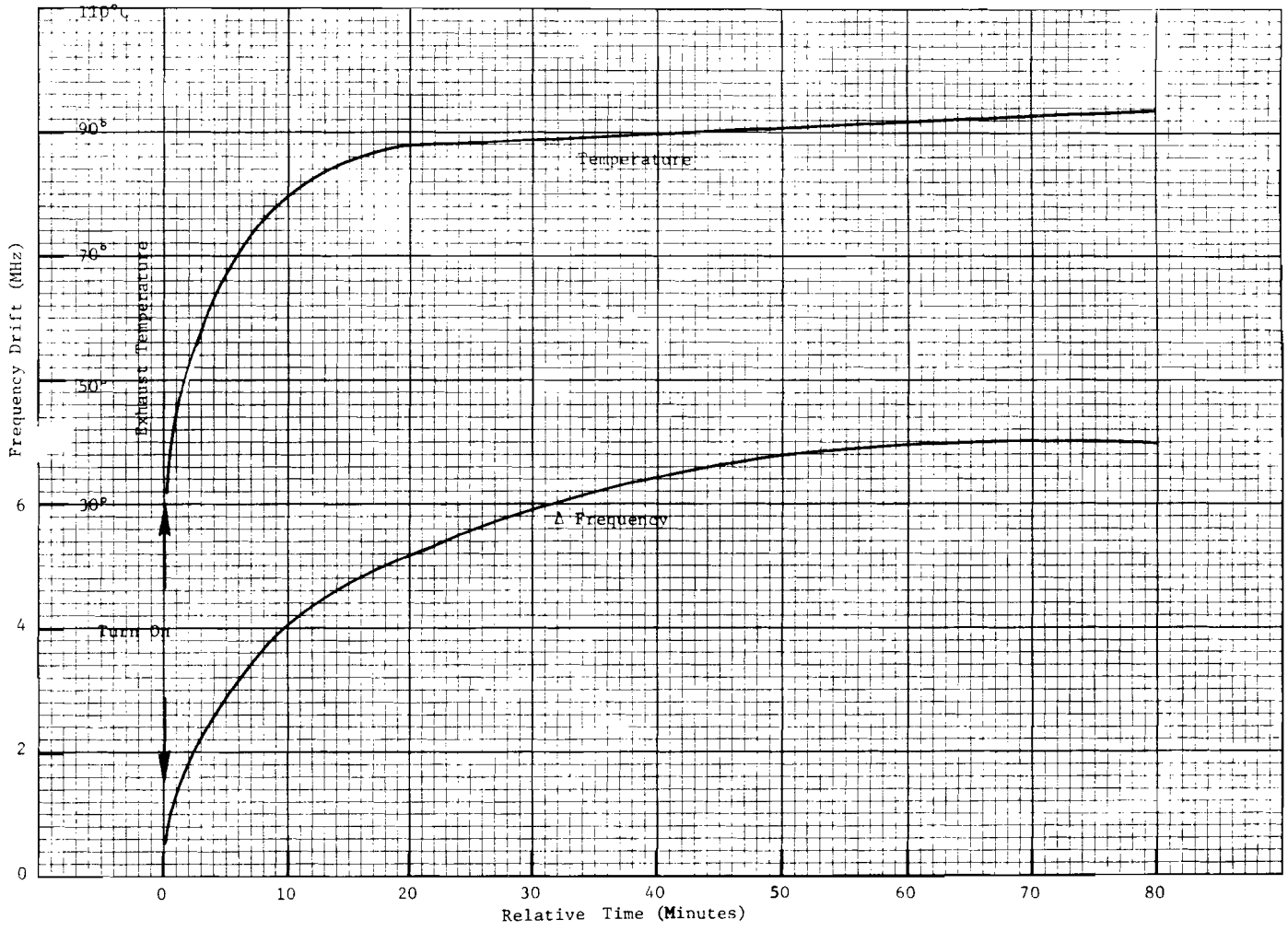

Fig. 11. Frequency drift and exhaust temperature rise of conventional magnetron (DX-276); ASR-7 normal operating conditions.

transistion, then through a 3-ft section of WR112, WR187 or WR90 waveguide, then back to coax and, thence to the spectrum analyzer.

Measurement of spurious responses from waveguide cutoff to 18 GHz requires that the pick-off, probe, directional coupler or whatever attenuates the signal to the analyzer, have a flat frequency response over this region. No such device is available. Complicating the problem is the existence of high order modes in the S-band waveguide at the upper frequencies. In order to simplify the problem, a small capacitive probe was used to sample the electric field in the waveguide. Ignoring higher order modes, such a probe would be expected to have an attenuation inversely proportional to frequency. The probe was calibrated by inserting two identical probes in the waveguide and measuring the attenuation between the two as a function of frequency. A scattering of values was obtained as shown in Figure 12. The attenuation of one probe is then assumed to be half (in dB) the attenuation of both. A best fit straight line approximation shows the one-way attenuation to go as $(f)^{-1.28}$, which is approximately inversely proportional to frequency. An approximate probe correction formula can be inferred from Figure 12, i.e.

$$c = 25.6 \log_{10} f - 11.5 \pm 5$$

where c is the additional sensitivity (in dB) one has as a function of frequency f (in GHz). Thus, at 18 GHz the spectra are 20.6 dB more sensitive, making the 60 dB below the main lobe level really 80.6 dB below the main lobe.

2. Spectra of Magnetron Spurious Responses

The table given below indexes sets of figures showing photographs of the spurious responses obtained on each magnetron at low, mid and upper test frequencies. The caption block on the face of each spectrum photograph identifies the frequency at the center of the analyzer screen (f_c), the relative gain setting (G_{rel}) and the level of harmonic energy if present. Conditions under which each spurious response spectrum was photographed are identical to those for the previously numbered spectrum figure except for the conditions noted in the individual figure captions.

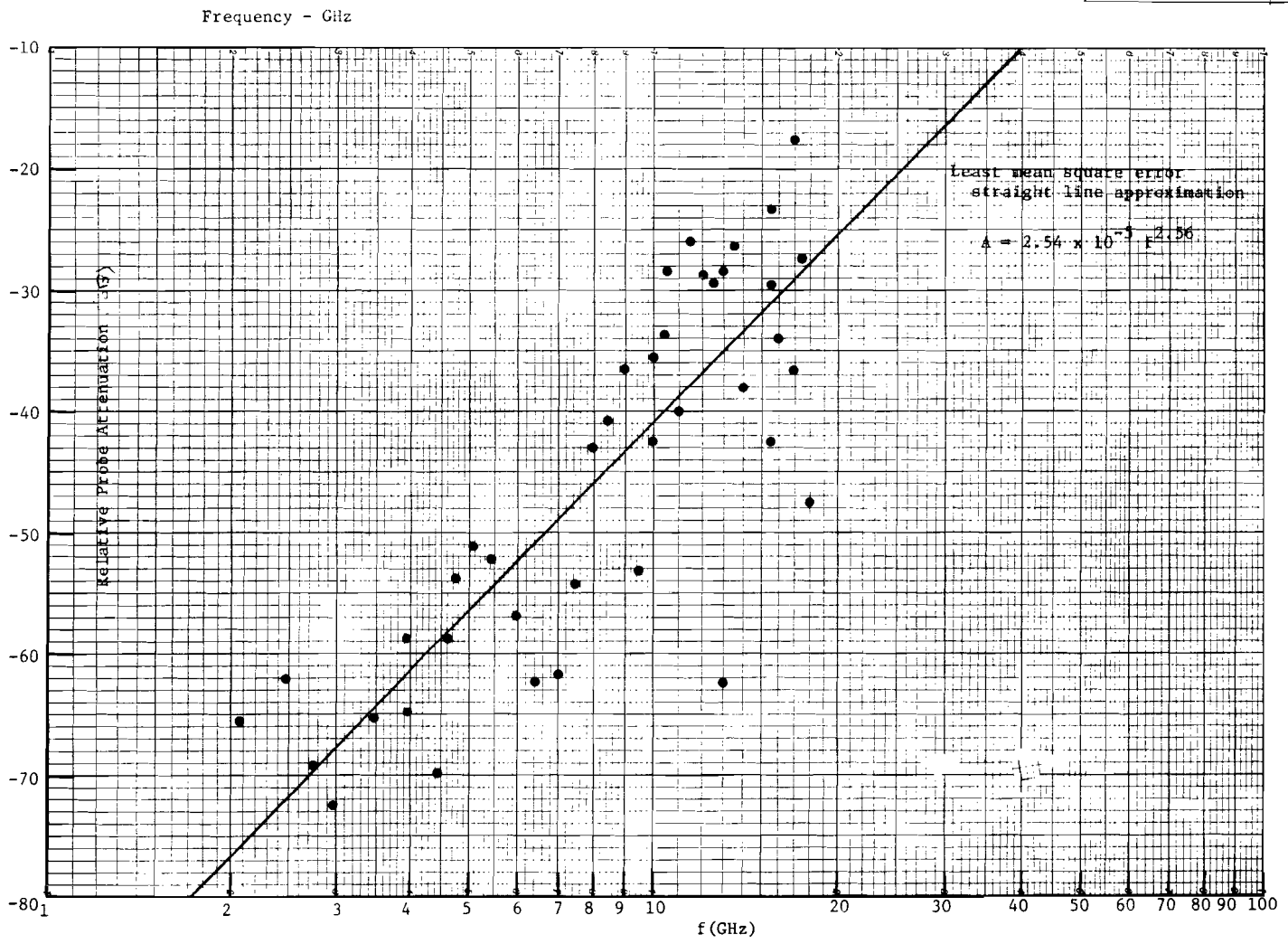

Fig. 12. Two-way probe attenuation vs frequency.

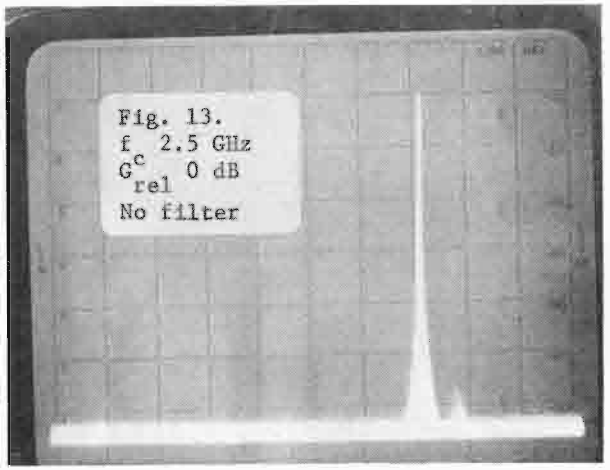

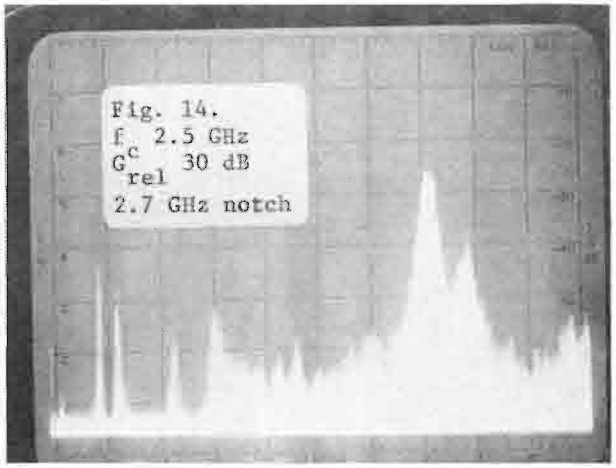

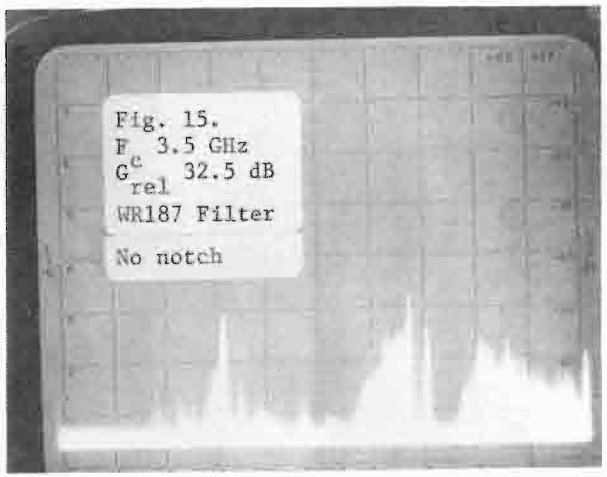

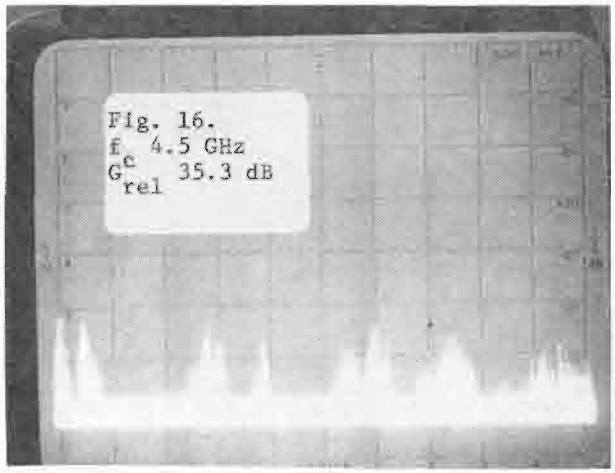

Figs. 13-16. Coaxial magnetron (QKH-1739LL) operated at 2.7 GHz (V-axis: 10 dB/div; H-axis: 100 MHz/div).

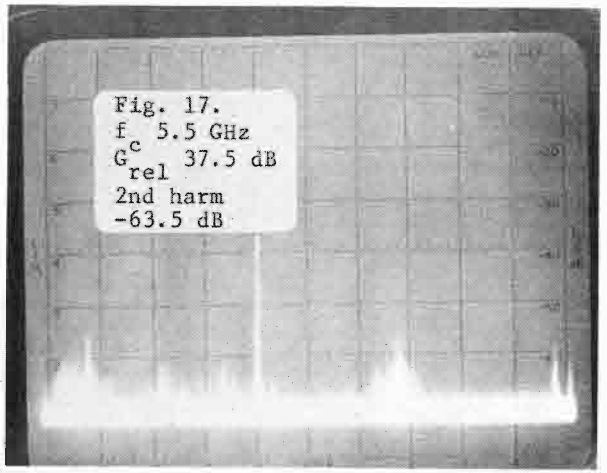

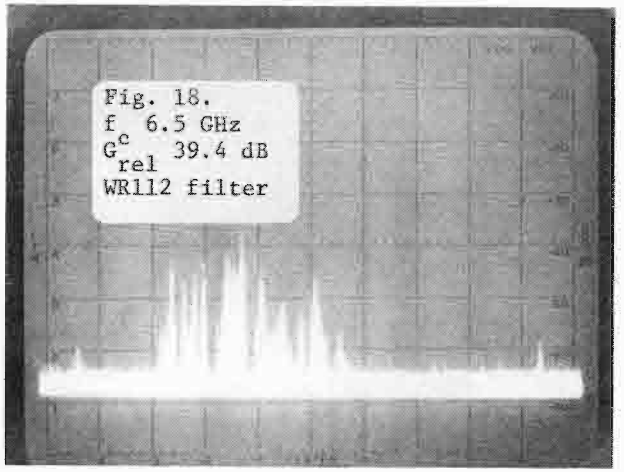

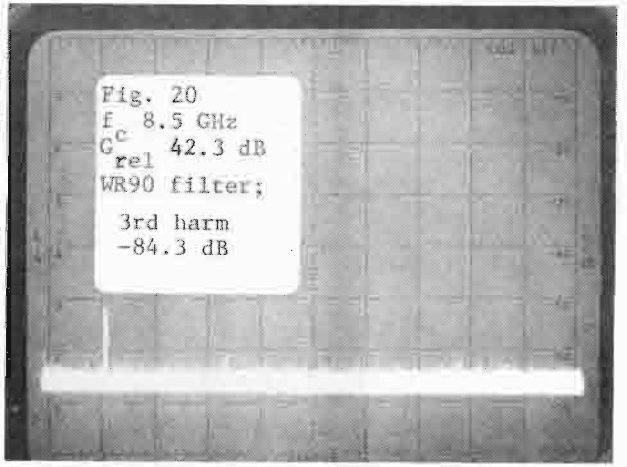

Figs. 17-20. Coaxial magnetron (QKH-1739LL) operated at 2.7 GHz (V-axis: 10 dB/div; H-axis: 100 MHz/div).

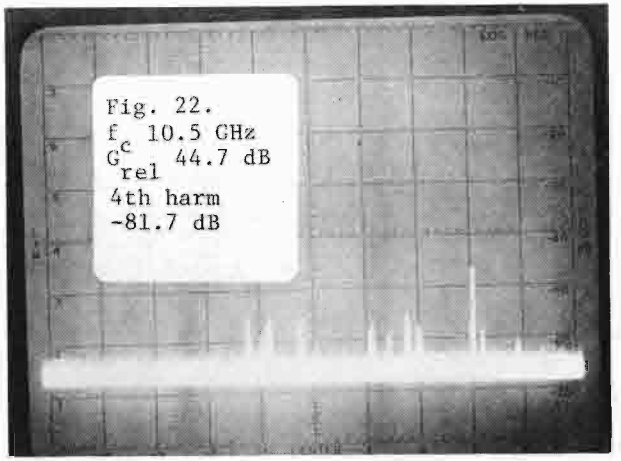

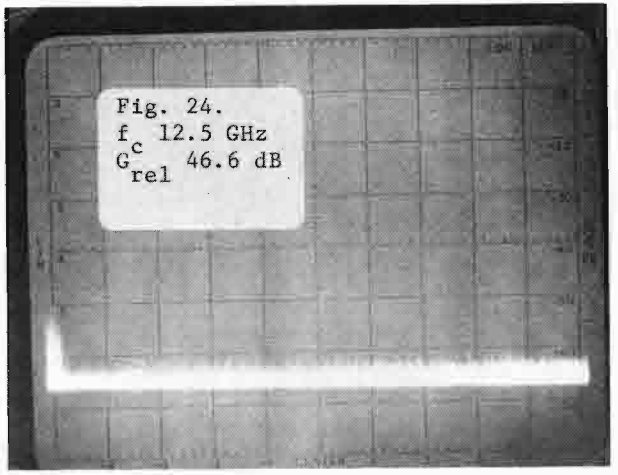

Figs. 21-24. Coaxial magnetron (QKH-1739LL) operated at 2.7 GHz (V-axis: 10 dB/div; H-axis: 100 MHz/div).

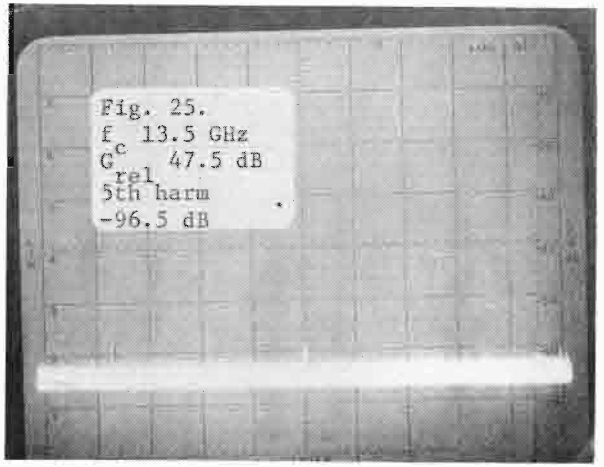

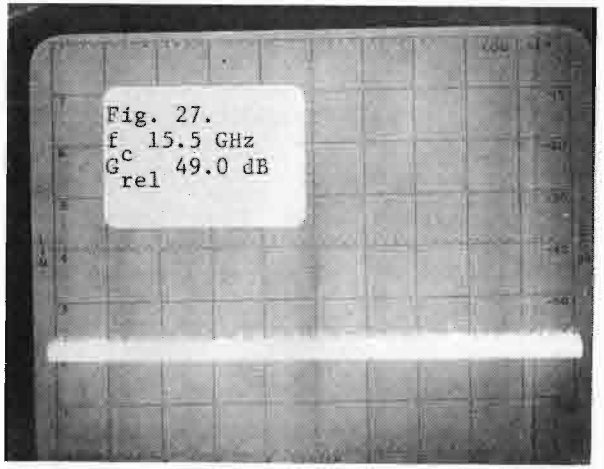

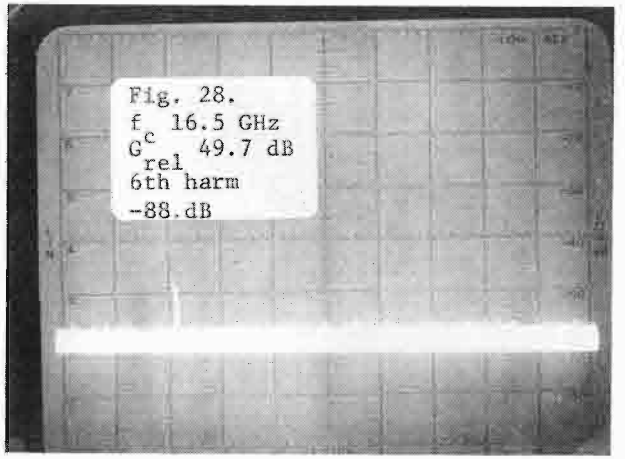

Figs. 25-28. Coaxial magnetron (QKH-1739LL) operated at 2.7 GHz (V-axis: 10 dB/div; H-axis: 100 MHz/div).

ATC-74(29)

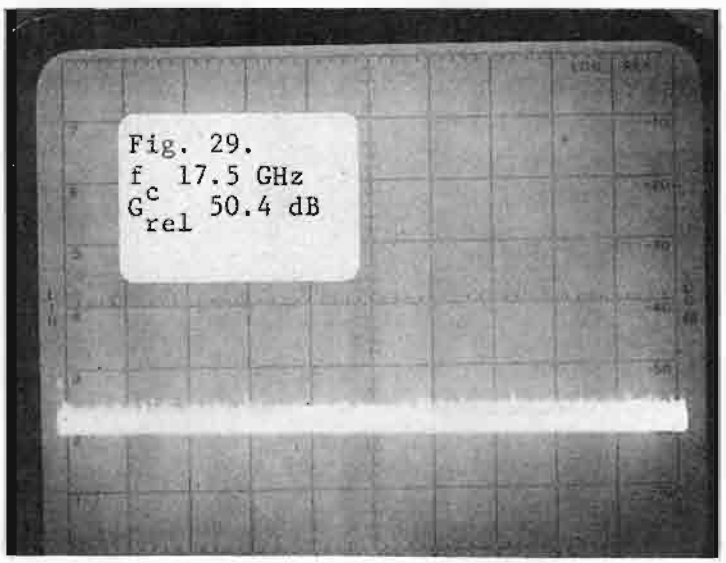

Fig. 29. Coaxial magnetron (QKH-1739LL) operated at 2.7 GHz (V-axis: 10 dB/div; H-axis: 100 MHz/div).

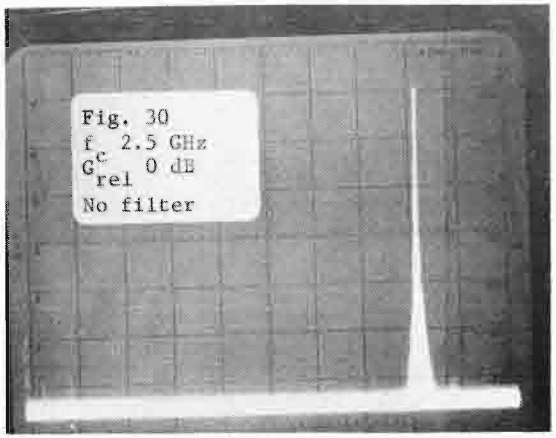

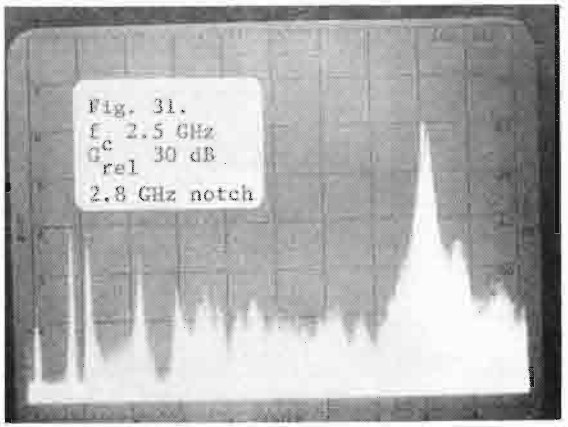

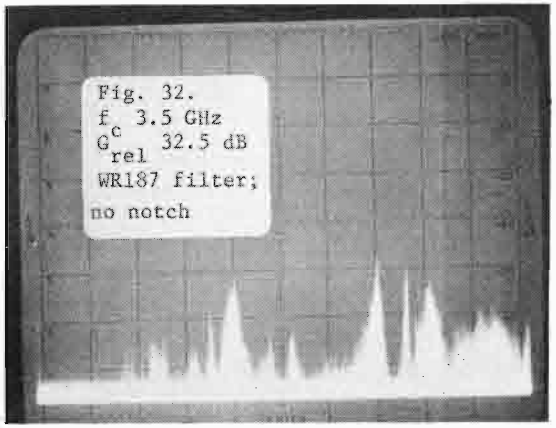

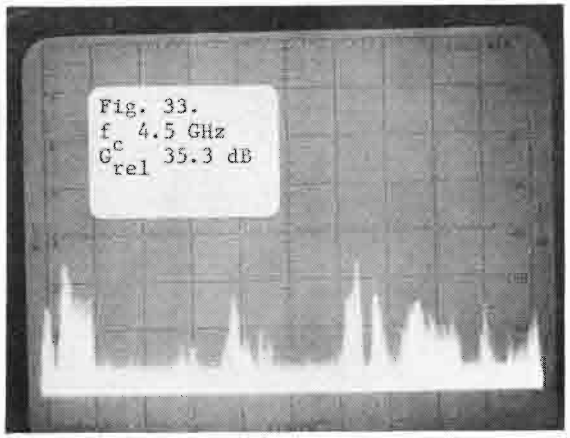

Figs. 30-33. Coaxial magnetron (QKH-1739LL) operated at 2.8 GHz (V-axis: 10 dB/div; H-axis: 100 MHz/div).

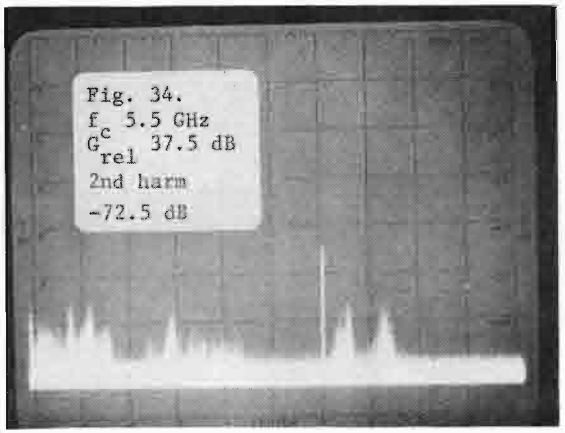

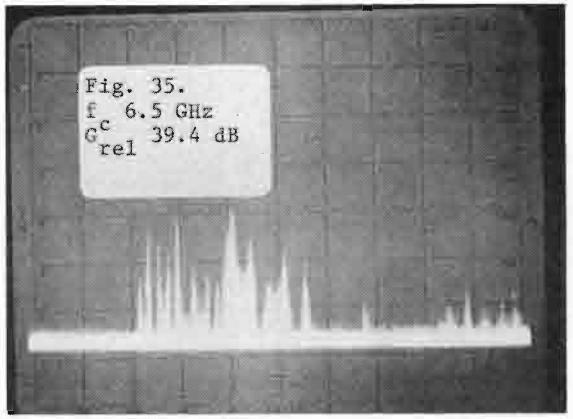

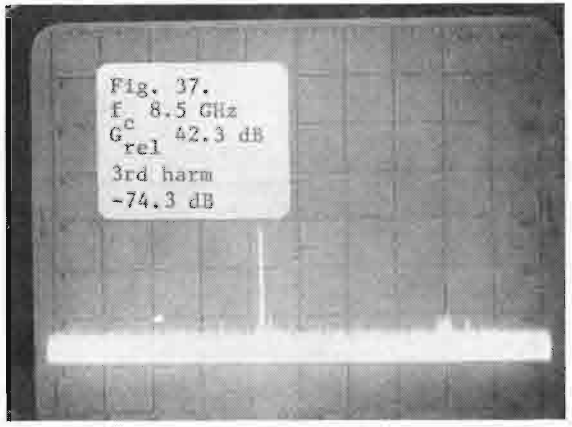

Figs. 34-37. Coaxial magnetron (QKH-1739 LL) operated at 2.8 GHz (V-axis: 10 dB/div; H-axis: 100 MHz/div).

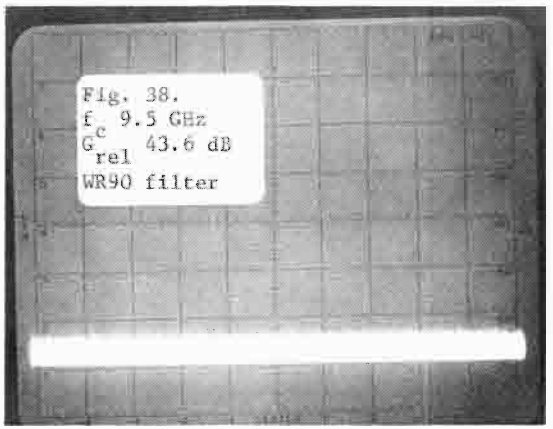

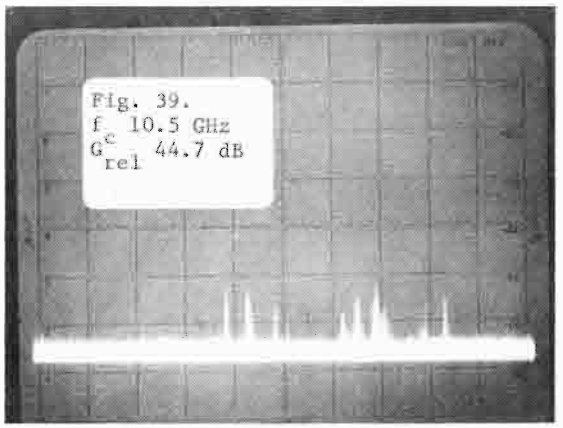

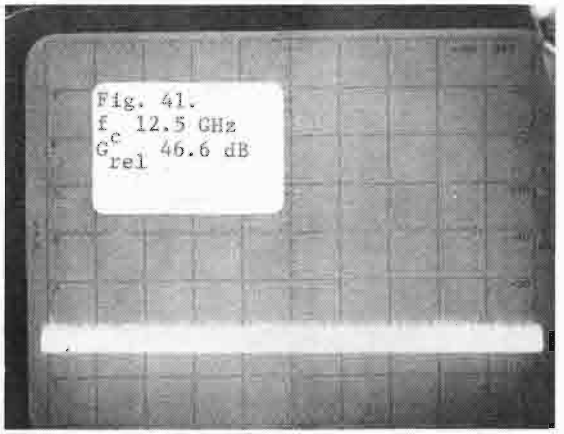

Figs. 38-41. Coaxial magnetron (QKH-1739LL) operated at 2.8 GHz (V-axis: 10 dB/div; H-axis: 100 MHz/div).

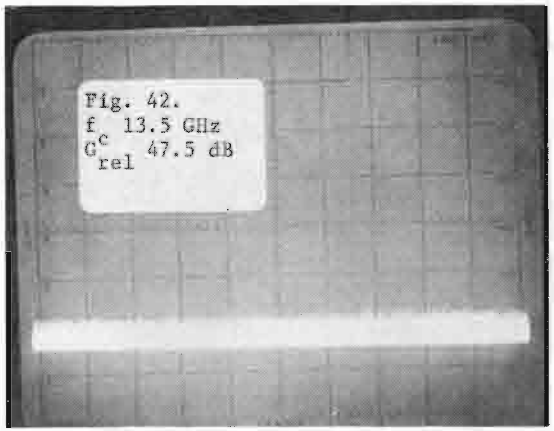

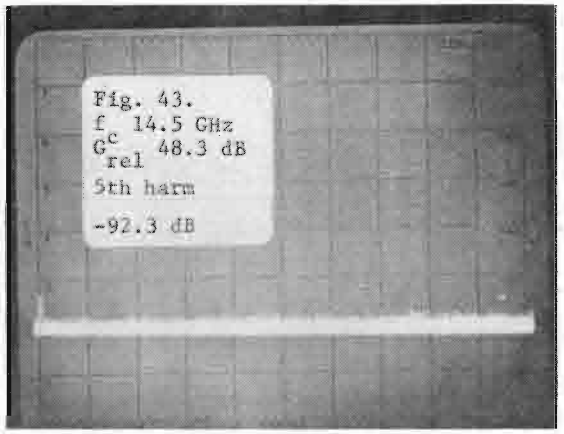

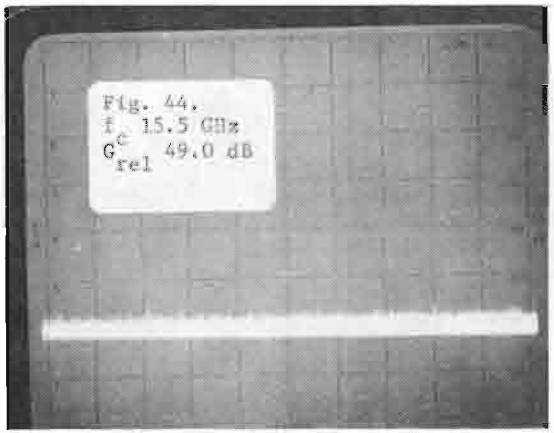

Figs. 42-45. Coaxial magnetron (QKH-1739LL) operated at 2.8 GHz (V-axis: 10 dB/div; H-axis: 100 MHz/div).

ATC-74(46)

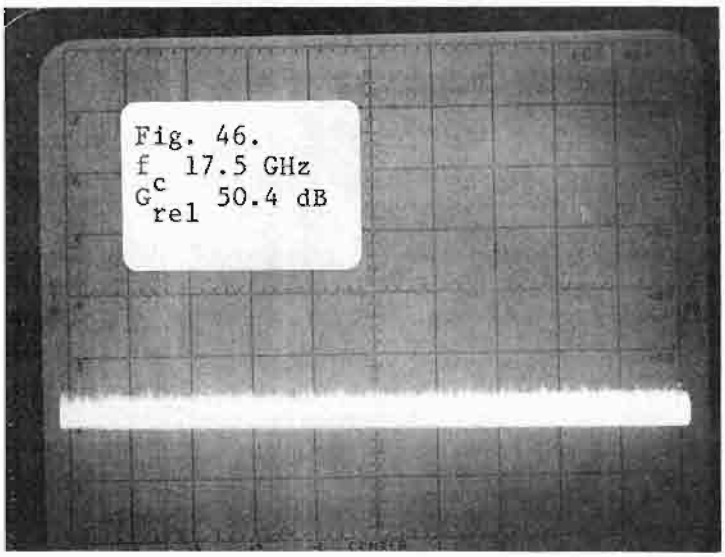

Fig. 46. Coaxial magnetron (QKH-1739LL) operated at 2.8 GHz (V-axis: 10 dB/div; H-axis: 100 MHz/div).

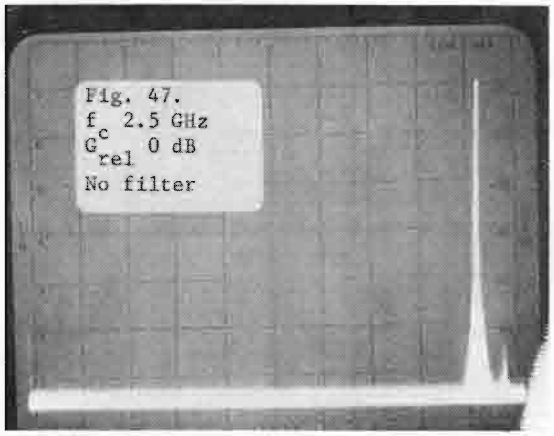

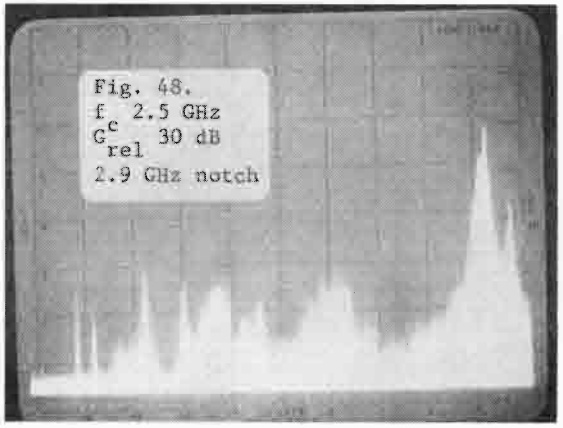

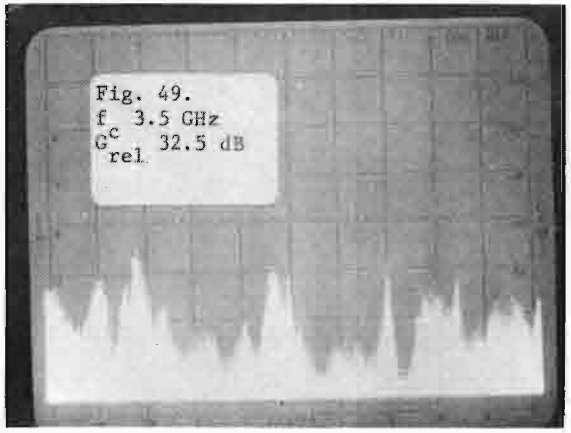

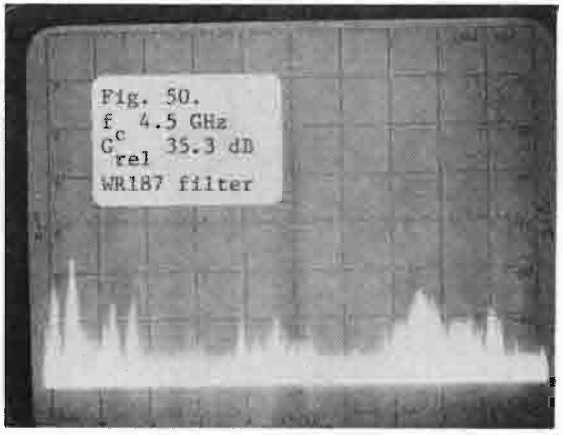

Figs. 47-50. Coaxial magnetron (QKH-1739LL) operated at 2.9 GHz (V-axis: 10 dB/div; H-axis: 100 MHz/div).

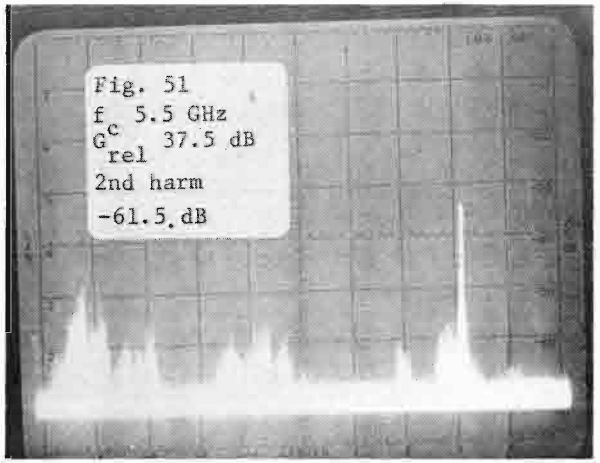

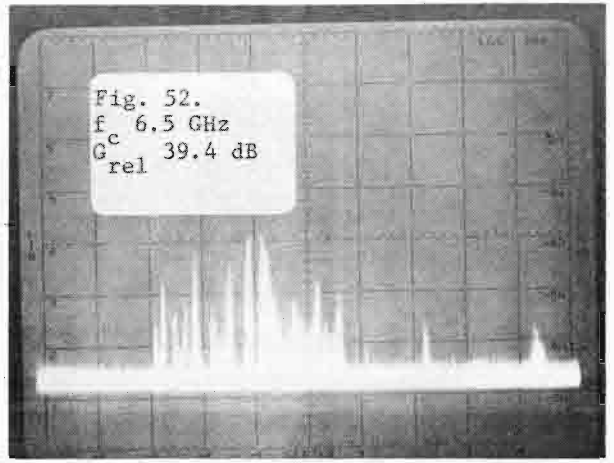

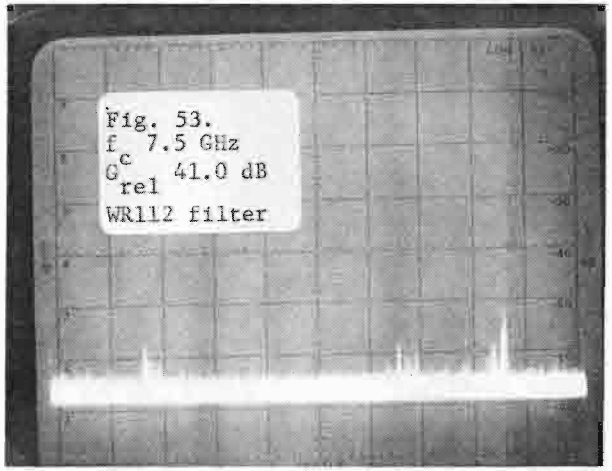

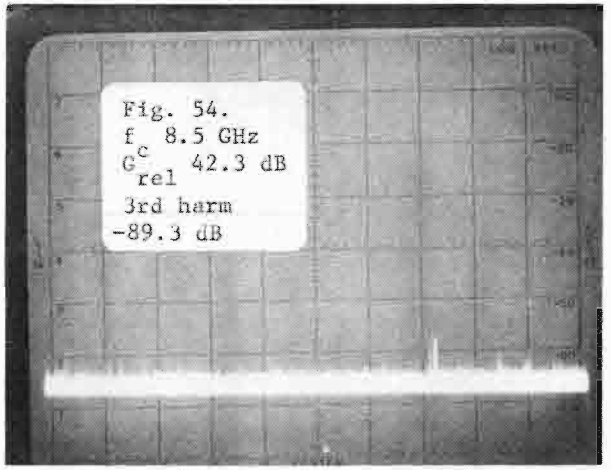

Figs. 51-54. Coaxial magnetron (QKH-1739LL) operated at 2.9 GHz (V-axis: 10 dB/div; H-axis: 100 MHz/div).

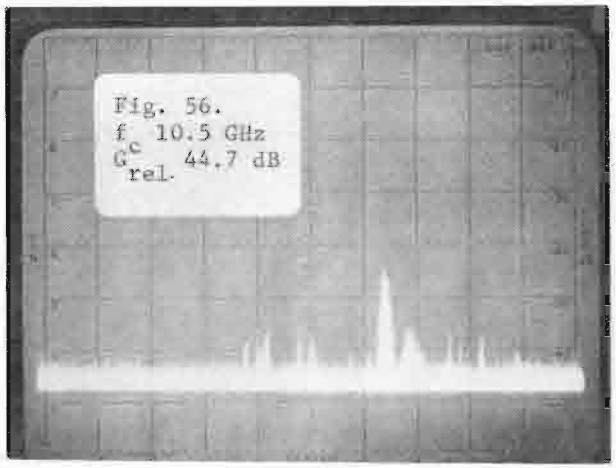

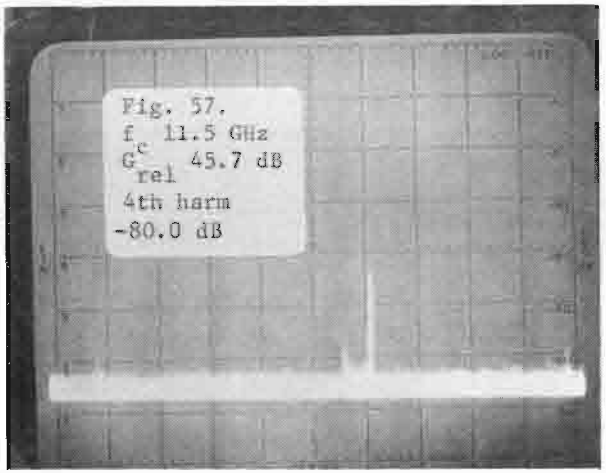

Figs. 55-58. Coaxial magnetron (QKH-1739LL) operated at 2.9 GHz (V-axis: 10 dB/div; H-axis: 100 MHz/div).

Figs. 59-62. Coaxial magnetron (QKH-1739LL) operated at 2.9 GHz (V-axis: 10 dB/div; H-axis: 100 MHz/div).

ATC-74(63)

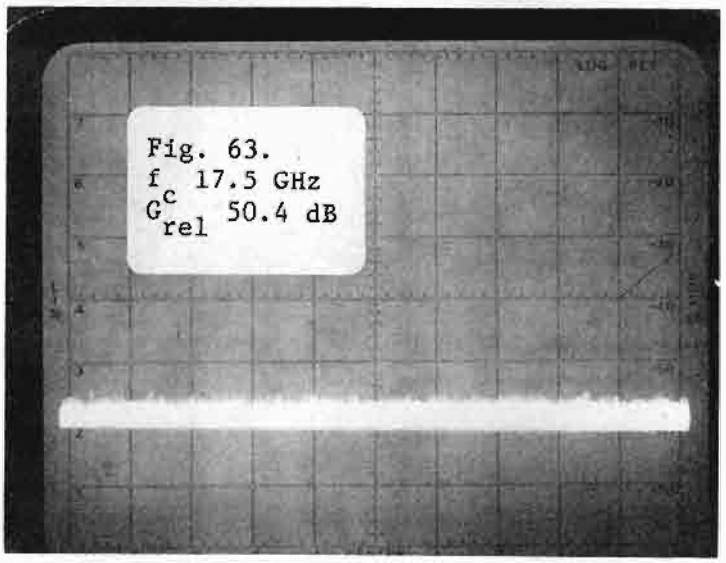

Fig. 63. Coaxial magnetron (QKH-1739LL) operated at 2.9 GHz (V-axis: 10 dB/div; H-axis: 100 MHz/div).

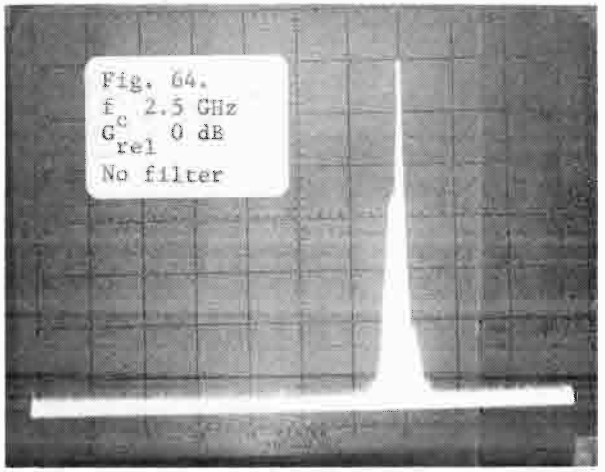

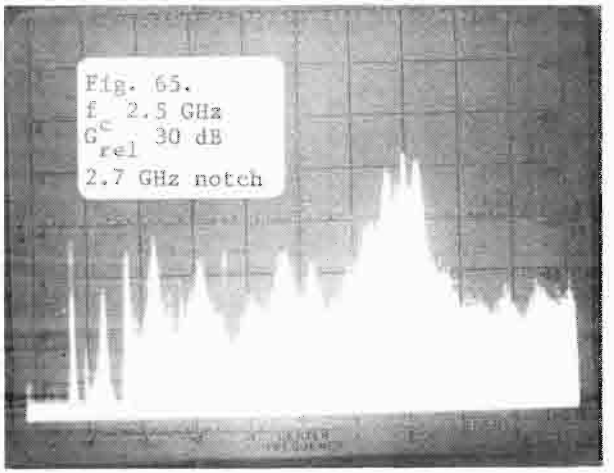

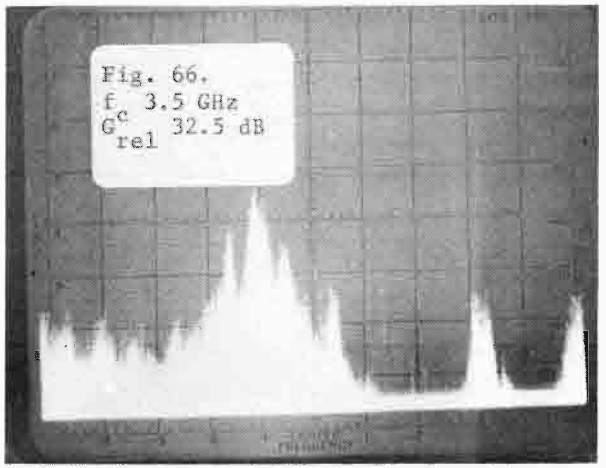

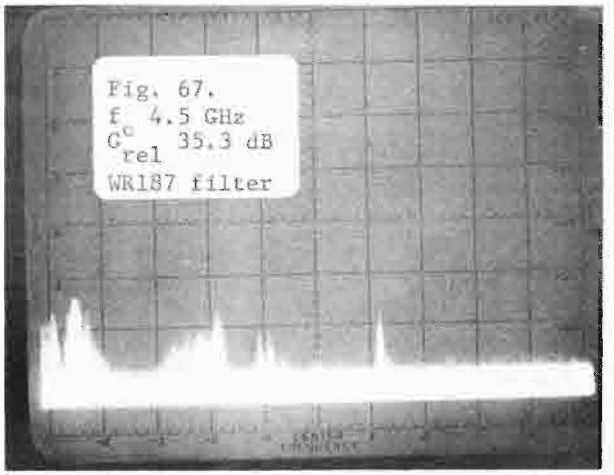

Figs. 64-67. Conventional magnetron (DX-276) operated at 2.7 GHz (V-axis: 10 dB/div; H-axis: 100 MHz/div).

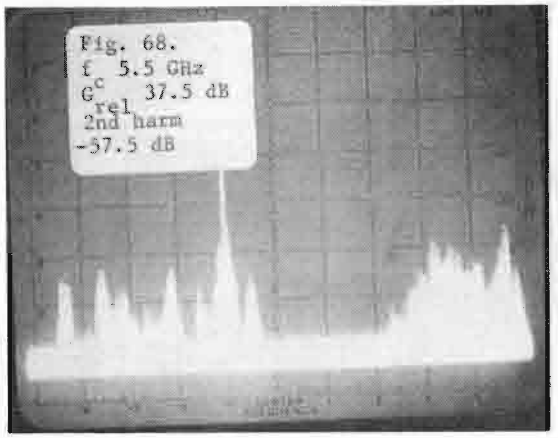

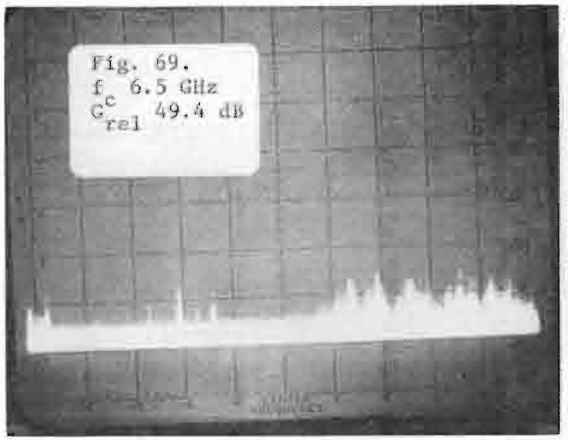

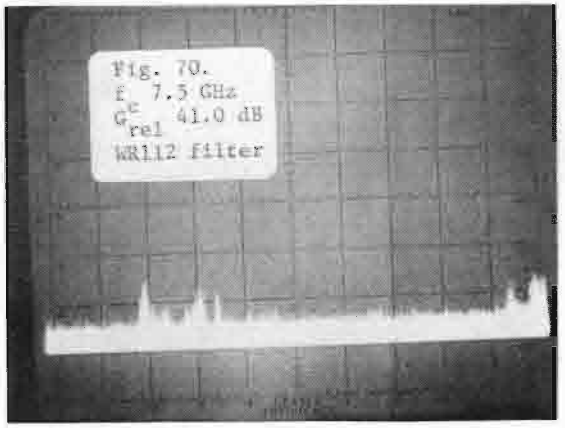

Figs. 68-71. Conventional magnetron (DX-276) operated at 2.7 GHz (V-axis: 10 dB/div; H-axis: 100 MHz/div).

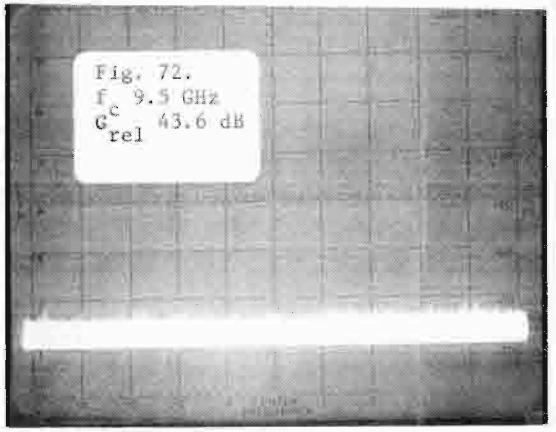

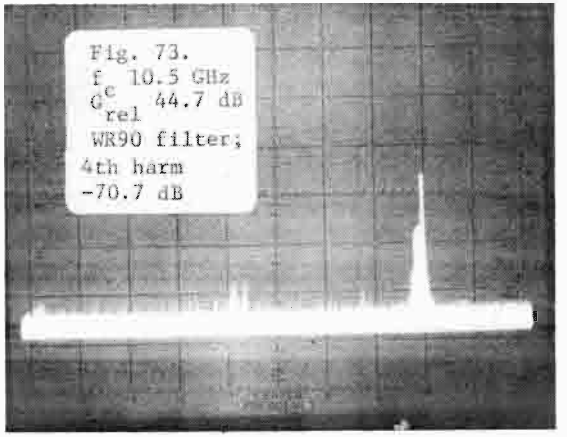

Figs. 72-75. Conventional magnetron (DX-276) operated at 2.7 GHz (V-axis: 10 dB/div; H-axis: 100 MHz/div).

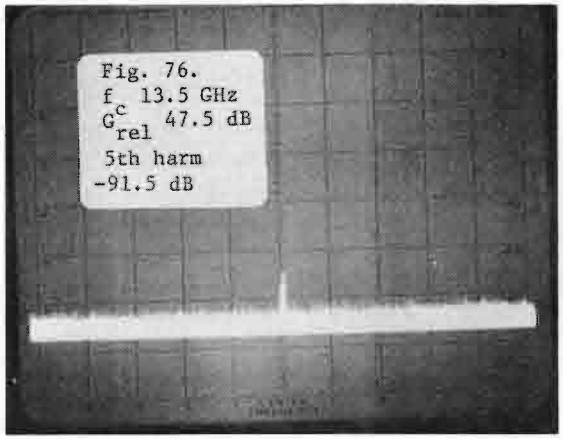

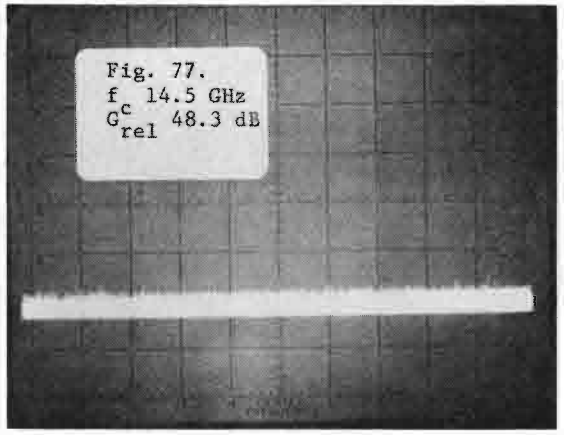

Figs. 76-79. Conventional magnetron (DX-276) operated at 2.7 GHz (V-axis: 10 dB/div; H-axis: 100 MHz/div).

ATC-74(80)

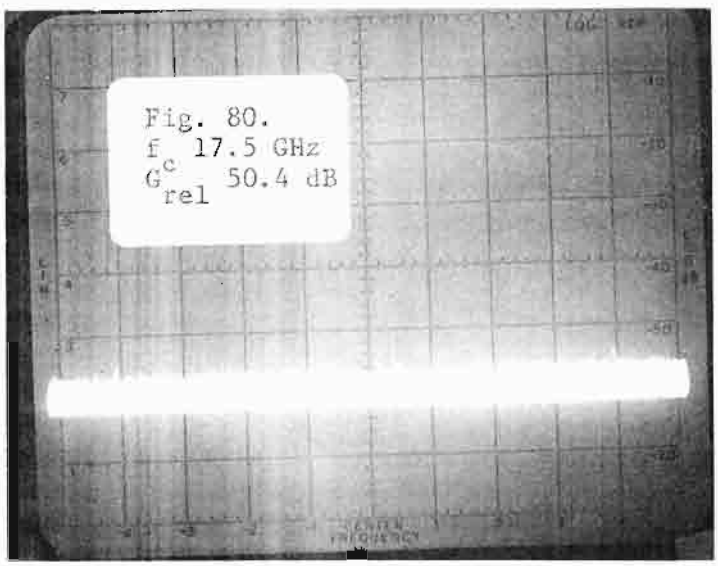

Fig. 80. Conventional magnetron (DX-276) operated at 2.7 GHz (V-axis: 10 dB/div; H-axis: 100 MHz/div).

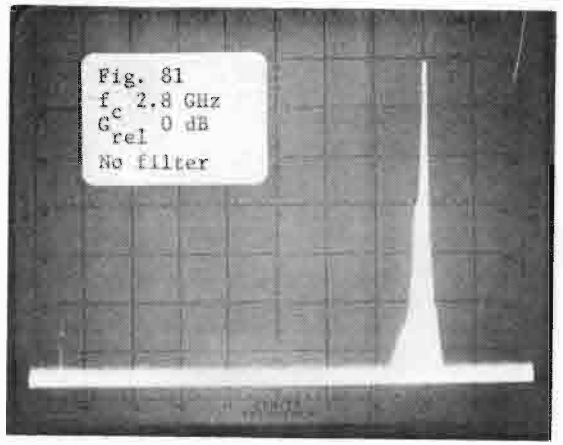

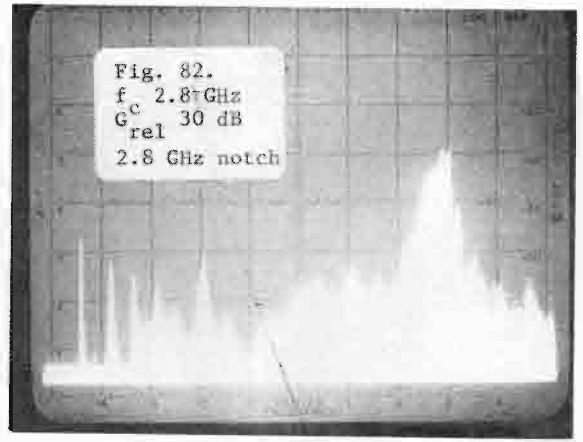

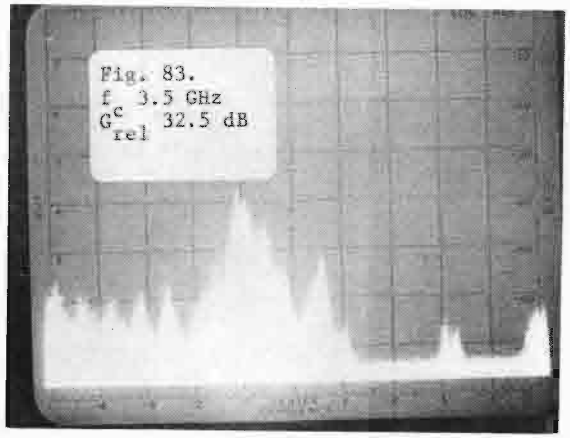

Figs. 81-84. Conventional magnetron (DX-276) operated at 2.8 GHz (V-axis: 10 dB/div; H-axis: 100 MHz/div).

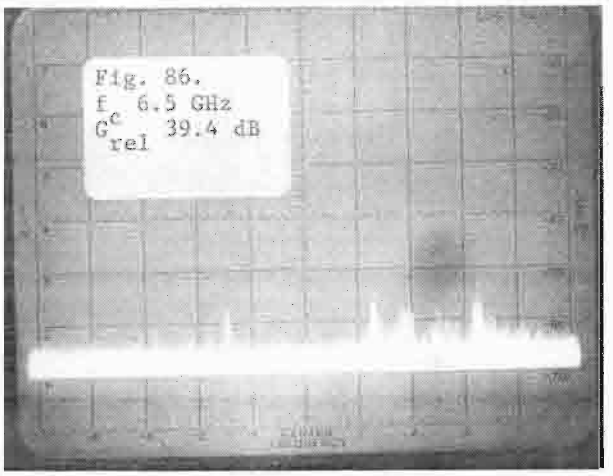

Figs. 85-88, Conventional magnetron (DX-276) operated at 2.8 GHz (V-axis: 10 dB/div; H-axis: 100 MHz/div).

Figs. 89-92. Conventional magnetron (DX-276) operated at 2.8 GHz (V-axis: 10 dB/div; H-axis: 100 MHz/div).

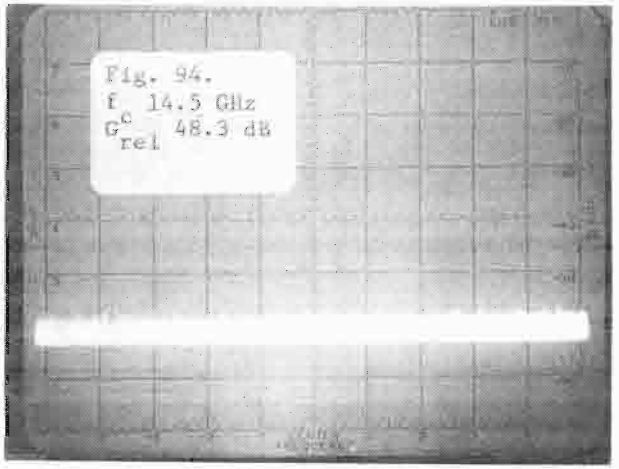

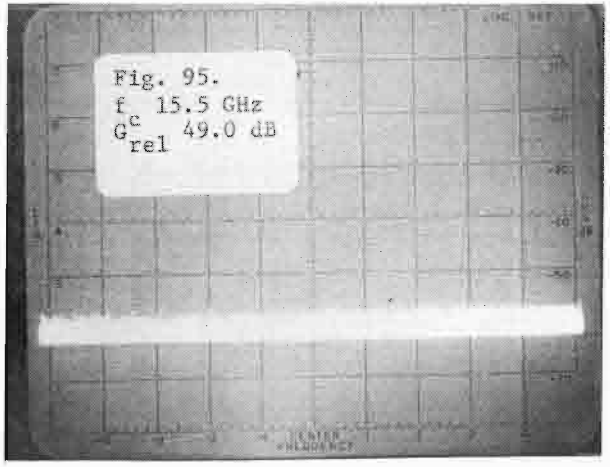

Figs. 93-96. Conventional magnetron (DX-276) operated at 2.8 GHz (V-axis: 10 dB/div; H-axis: 100 MHz/div).

ATC-74(97)

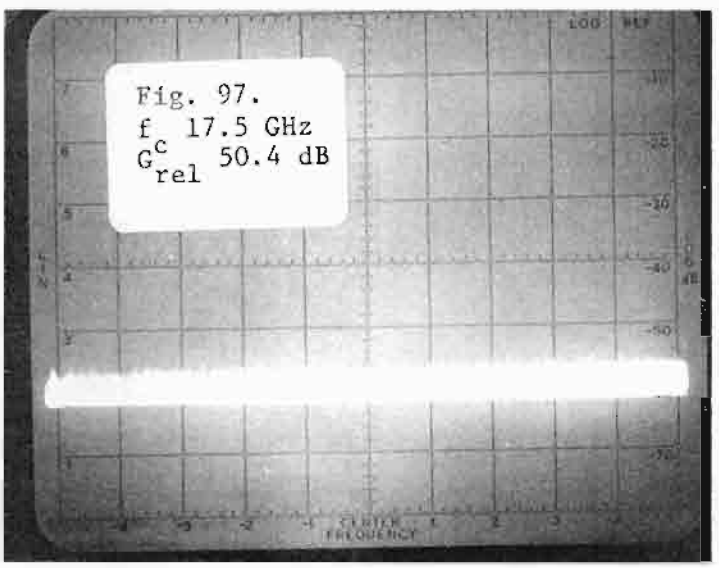

Fig. 97. Conventional magnetron (DX-276) operated at 2.8 GHz (V-axis: 10 dB/div; H-axis: 100 MHz/div).

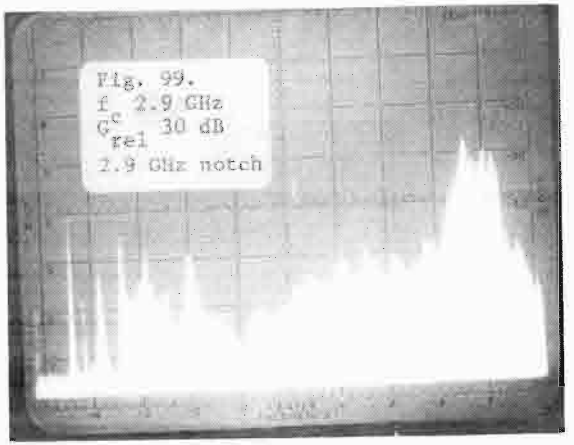

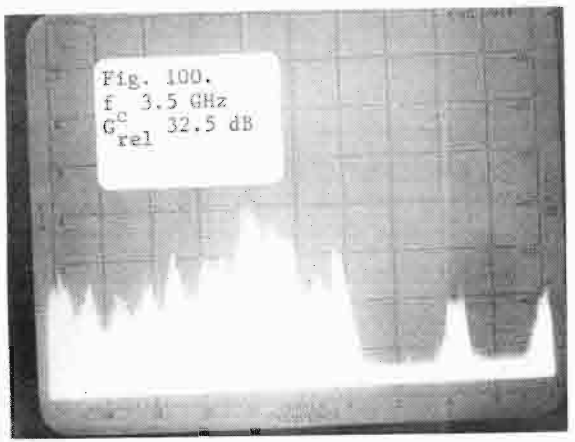

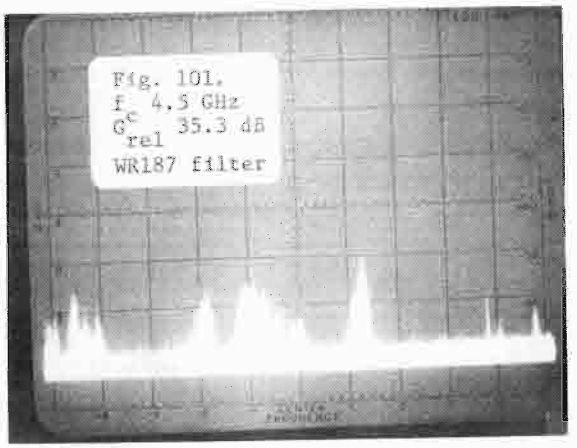

Figs. 98-101. Conventional magnetron (DX-276) operated at 2.9 GHz (V-axis: 10 dB/div; H-axis: 100 MHz/div).

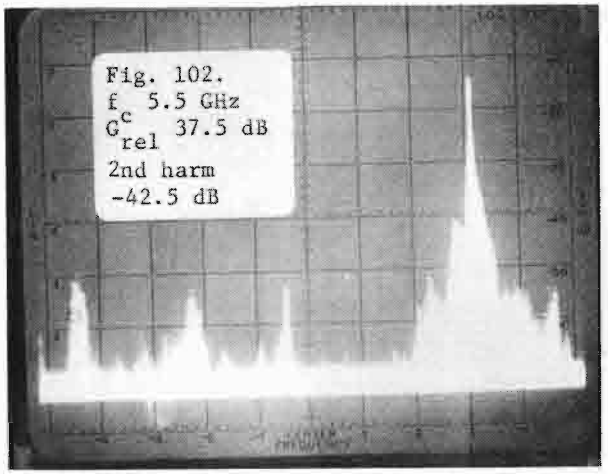

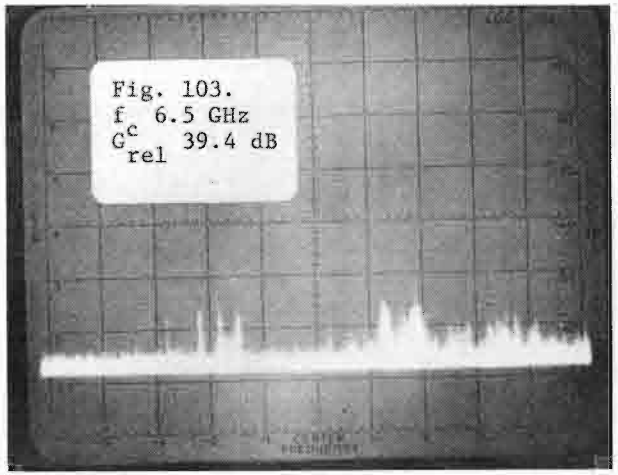

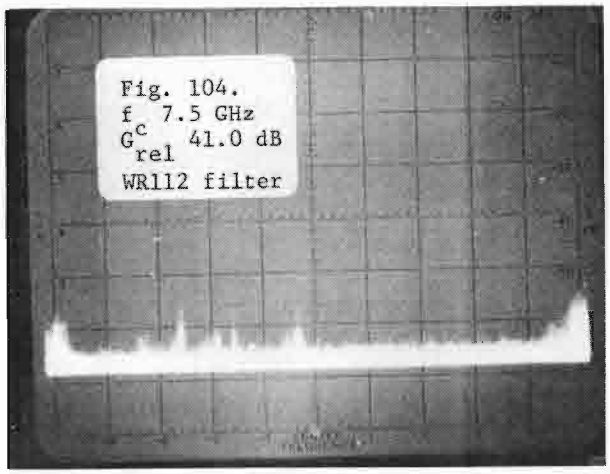

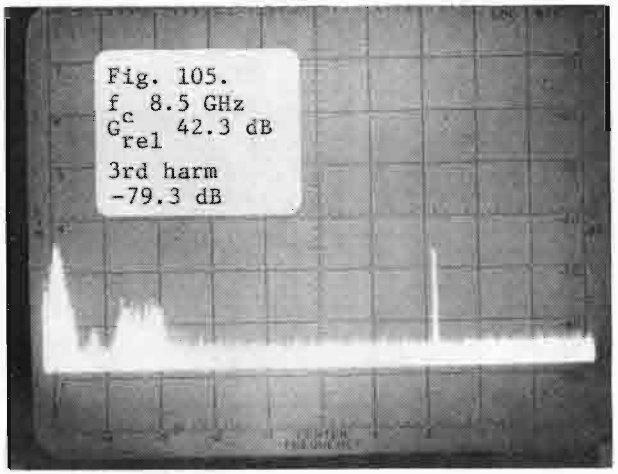

Figs. 102-105. Conventional magnetron (DX-276) operated at 2.9 GHz (V-axis: 10 dB/div; H-axis: 100 MHz/div).

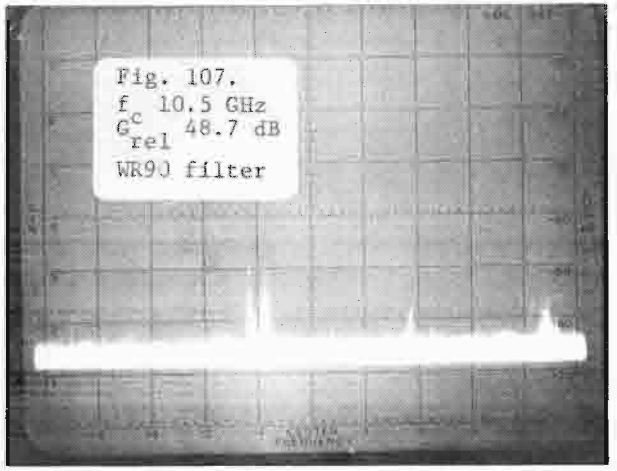

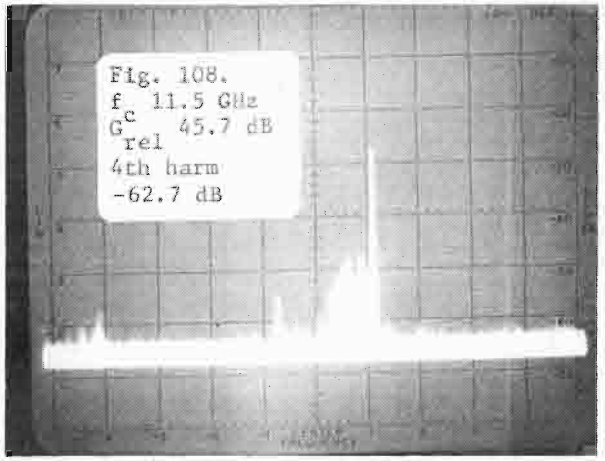

Figs. 106-109. Conventional magnetron (DX-276) operated at 2.9 GHz (V-axis: 10 dB/div; H-axis: 100 MHz/div).

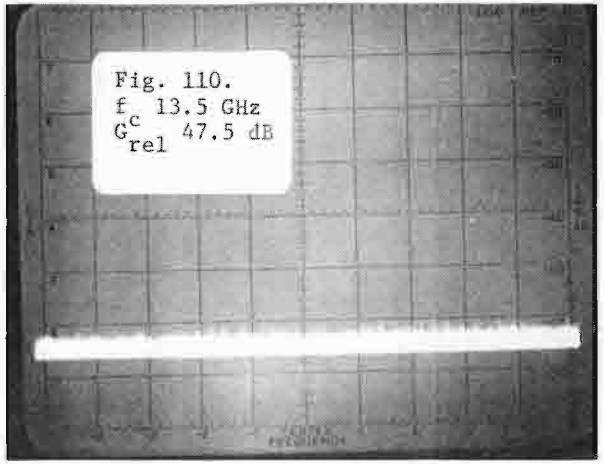

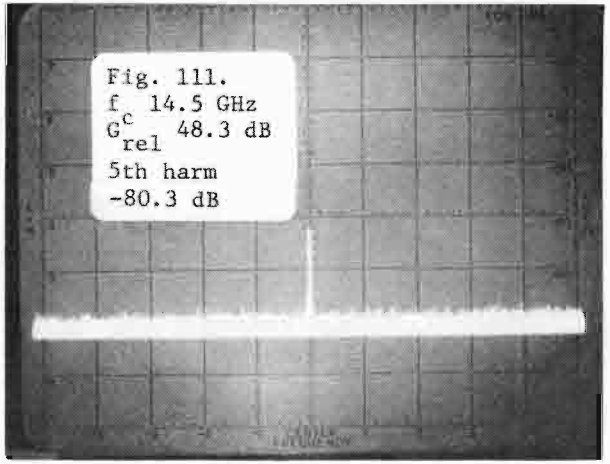

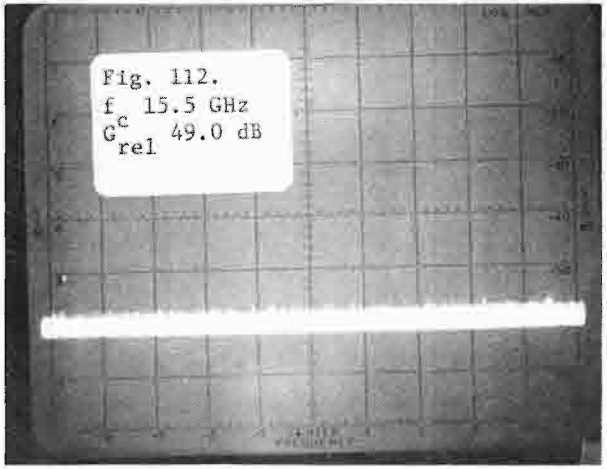

Figs. 110-113. Conventional magnetron (DX-276) operated at 2.9 GHz (V-axis: 10 dB/div; H-axis: 100 MHz/div).

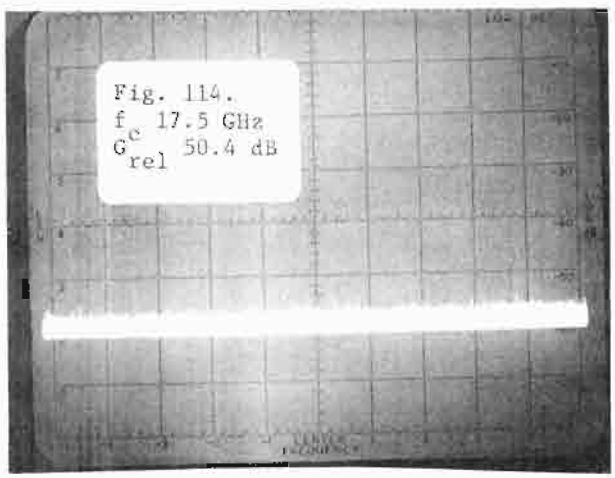

Fig. 114. Conventional magnetron (DX-276) operated at 2.9 GHz (V-axis: 10 dB/div; H-axis: 100 MHz/div).

Magnetron	Figures Numbered 2.7 GHz	2.8 GHz	2.9 GHz
Coaxial (QKH-1739LL)	13 thru 29	30 thru 46	47 thru 63
Conventional (DX276)	64 thru 80	81 thru 97	98 thru 114

D. Coaxial Magnetron Pulse Jitter

1. Measurement of Time Jitter

Conventional magnetrons have a small amount of time jitter compared to coaxial magnetrons. The amount of jitter is generally so small as to have little effect in most radar applications. Because the jitter is small and because of the difficulty of measuring such small time differences, only measurements of the coaxial magnetron were made.

Figure 115 shows the RF envelope of the QK1739LL coaxial magnetron as viewed on a sampling oscilloscope under the following conditions.

(1) The standard diode network controlling the rate of rise was used (as described in Section II).

(2) A 2-watt RF pulsed signal was injected into the magnetron during the turn-on time of the modulator pulse to the magnetron. The RF circuit is shown in Figure 116.

In Figure 117 the front edge of the RF envelope is expanded to show the starting jitter with the priming signal. The scope is triggered from the front edge of the applied modulator voltage pulse. The jitter is estimated to have a standard deviation of 3 nsecs. Without priming (Figure 118), the jitter deviation increases to about 10 nsecs.

2. Effect of Pulse Shape Jitter

The effect of pulse shape jitter on the performance of an MTI radar is now discussed. A magnetron transmitter pulse that has pulse shape jitter may be analyzed by treating it as the sum of two pulses, a steady and a fluctuating pulse. The fluctuating component is uncorrelated (the magnetron has no memory) and will affect the MTI processor as white noise. The ratio of the steady component power to the noise power represents the maximum clutter-to-noise ratio that can be tolerated without reducing the radar sensitivity. It is necessary to calculate the noise-to-clutter ratio ϕ given an arbitrary jitter across the pulse.

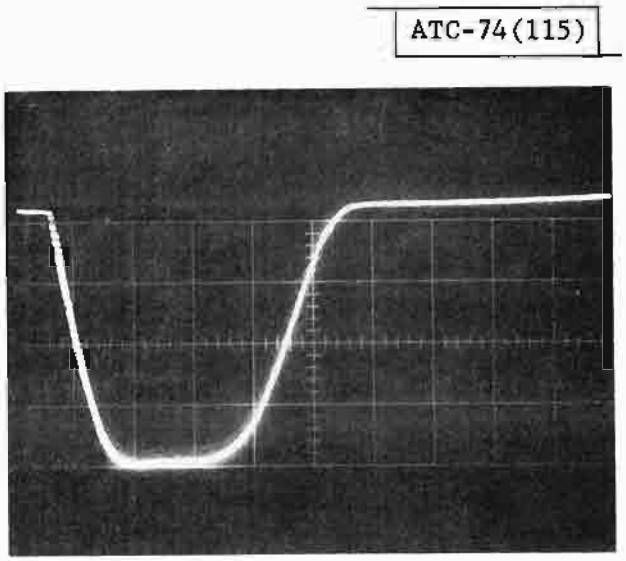

Fig. 115. RF envelope of coaxial magnetron as seen on a sampling scope (V-axis: linear power - not calibrated; H-axis: 0.2 μsec/div; pulse is 0.7 μsec long at half-power points).

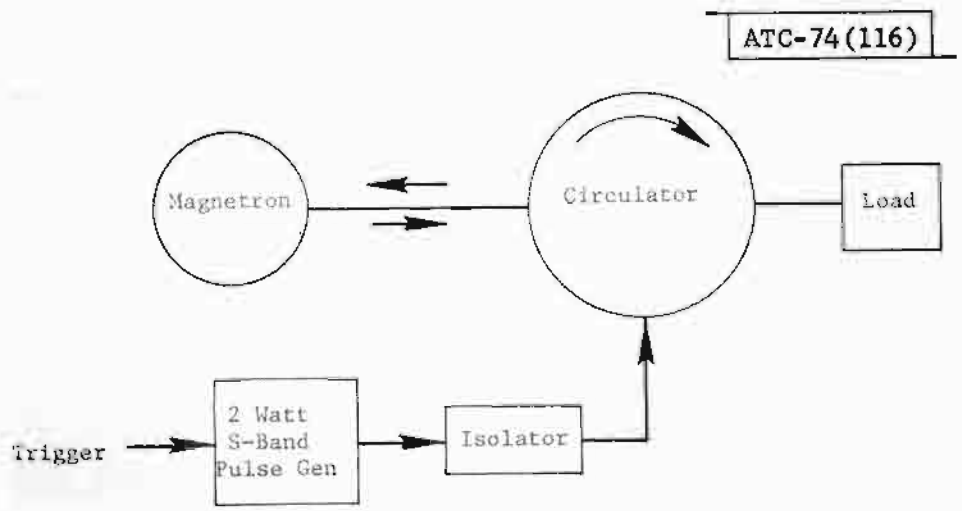

Fig. 116. Coaxial magnetron RF pulse injection.

ATC-74(117)

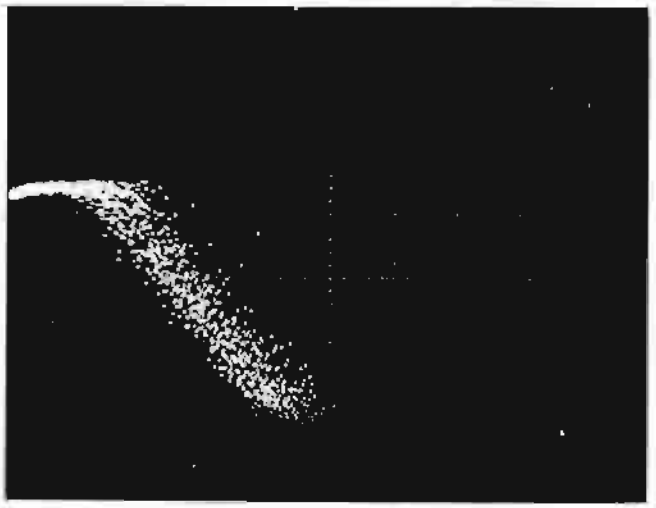

Fig. 117. Front edge of RF envelope - 2 watts of priming (V-axis: linear power - not calibrated; H-axis: 10 nsec/div).

ATC-74(118)

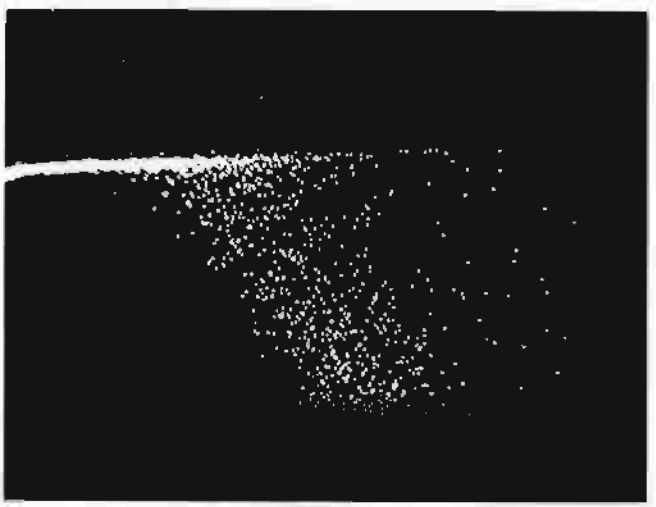

Fig. 118. Front edge of RF envelope - no priming (V-axis: linear power - not calibrated; H-axis: 10 nsec/div).

Let $V_n(t)$ represent the magnetron amplitude waveform of the nth pulse. $V_n(t)$ is a random variable. $\bar{V}(t)$ is defined as the mean of $V_n(t)$. The normalized clutter return from a point target is just

$$\int V^2(t)\, dt$$

while the residual noise caused by the jitter is

$$\int E\{(V_n(t) - \bar{V}(t))^2\}\, dt \qquad (4)$$

where the integrals are taken over the pulse and $E\{\ \}$ is the expectation operator. Thus, the noise-to-clutter ratio is

$$\phi = \frac{\int \sigma_v^2(t)\, dt}{\int V^2(t)\, dt} \qquad (5)$$

where

σ_v^2 is by definition the variance of V. Since $V^2(t) \simeq \bar{V}^2(t)$, the denominator is simply the peak power times the pulse length. The numerator is more involved. $\sigma_v^2(t)$ is greatest at the beginning of the pulse (Figure 119) and tapers to zero at t_o = 125 nsec. Unfortunately, $\sigma_v^2(t)$ cannot be estimated directly from Figure 119. This is because these pictures are of the output of a square-law detector and represent power.

Looking at Figure 117 and 119, one can represent the time jitter (standard deviation) as linearly decreasing

$$\sigma_t(t) = \sigma_{ot}\left(1 - \frac{t}{t_o}\right) \qquad 0 < t < t_o \qquad (6)$$

$$\sigma_t = 0 \qquad t_o < t$$

where σ_{ot} is the initial time jitter and t_o is the time when the jitter vanishes.

If one lets the normalized power be represented by

$$\bar{p} = \bar{V}^2$$

then $\Delta p = 2\,\bar{V}\,\Delta V = 2\,\bar{p}^{1/2}\,\Delta V$

and

ATC-74(119)

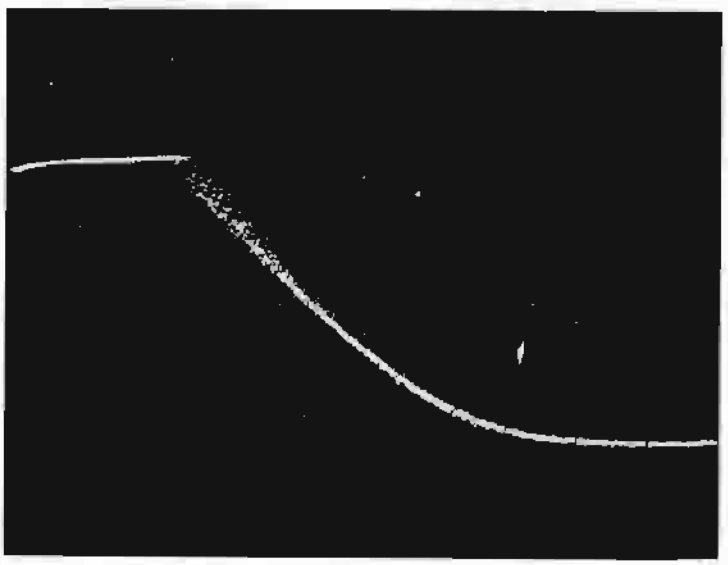

Fig. 119. Front edge of RF envelope - no priming (V-axis: linear power - not calibrated; H-axis: 50 nsec/div).

$$\sigma_p(t) = 2\,\bar{p}^{1/2}\,\sigma_v(t) \qquad \sigma_v << \bar{p}^{1/2} \qquad (7)$$

From Figure 119 one sees that

$$\bar{p} = m\,t \qquad 0 < t < t_o \qquad (8)$$

where m is the rise time slope. Thus,

$$\sigma_p(t) = m\,\sigma_t(t) \qquad 0 < t < t_o \qquad (9)$$

Combining (6), (7) and (8)

$$\sigma_v^2 = \frac{m}{4t}\,\sigma_{ot}^2\,(1 - \frac{t}{t_o})^2 \qquad 0 < t < t_o$$

Consequently, Eq. (5) becomes

$$\phi = \frac{\frac{m\,\sigma_{ot}^2}{4}\int_{t_o}^{t_o}(1 - \frac{t}{t_o})^2\,\frac{dt}{t}}{p_{max}\;\tau} \qquad (10)$$

where τ is the pulse length at the half power points. The integration cannot be taken from zero because of the pole at t = 0 and the requirement that $\sigma_v << \bar{p}^{1/2}$ (Eq. (7)). From Figure 117 and 118 one can estimate that

$\sigma_{ot} = 3 \times 10^{-9}$ sec with priming

$\sigma_{ot} = 10^{-8}$ sec without priming

and

$\tau = 7 \times 10^{-7}$ sec

$m = p_{max}/2.1 \times 10^{-7}$ watts/sec

Thus,

$\phi_{\text{timing jitter}} = -44$ dB (priming)

$\phi_{\text{timing jitter}} = -36$ dB (no priming)

This value can be compared to the value of ϕ caused by the coaxial magnetron frequency jitter. The value of ϕ obtained when the heater is optimally adjusted is

$$\phi_{\text{freq. jitter}} = -52 \text{ dB} \qquad (f_{\text{rms}} = 2 \text{ kc})$$

It would, therefore, appear that timing jitter is more of a problem than frequency jitter and that priming is necessary.

E. Pulling and Pushing Figures

The pushing figure experiment consists of applying square wave modulation to the high voltage pulse to the magnetron. The resultant peak-to-peak frequency current deviation constitutes the pushing figure. The frequency shifts were observed both on a spectrum analyzer and on a phase detector as in the frequency jitter tester. The current shifts were monitored on a scope by the use of a current transformer in the anode line to the magnetron. The pushing figures measured were:

Coaxial magnetron:	4.5 kHz/ampere
DX276:	31.0 kHz/ampere

Pulling figure is defined as the peak-to-peak frequency shift of the magnetron when the magnetron is subjected to 1.5 VSWR at all phase angles. The mismatch was generated by inserting a teflon slab into a longitudinal slot in the waveguide. By sliding the slab longitudinally in the slot all phases are generated. The pulling figures measured were:

Coaxial magnetron:	1.23 GHz at 2.80 GHz
DX276:	7.4 MHz at 2.86 GHz

F. Phase Locking the Coaxial Magnetron

Because priming the coaxial magnetron greatly reduces the timing jitter, it was thought that the priming signal could be used to phase lock the magnetron. In essence the magnetron would become an "amplifier" and one would have a coherent transmitter. Measurements of the rms phase error of the magnetron relative to the priming signal were made at four different priming powers (up to 6 kW). A plot of the rms phase error θ_{rms} (standard deviation) is shown in Figure 120. At 6 kW the θ_{rms} is 2.7 degrees. This corresponds to

$$\phi = 10 \log \left(\frac{\theta_{\text{rms}}}{360} \times 2\pi\right)^2 = -26.5 \text{ dB}$$

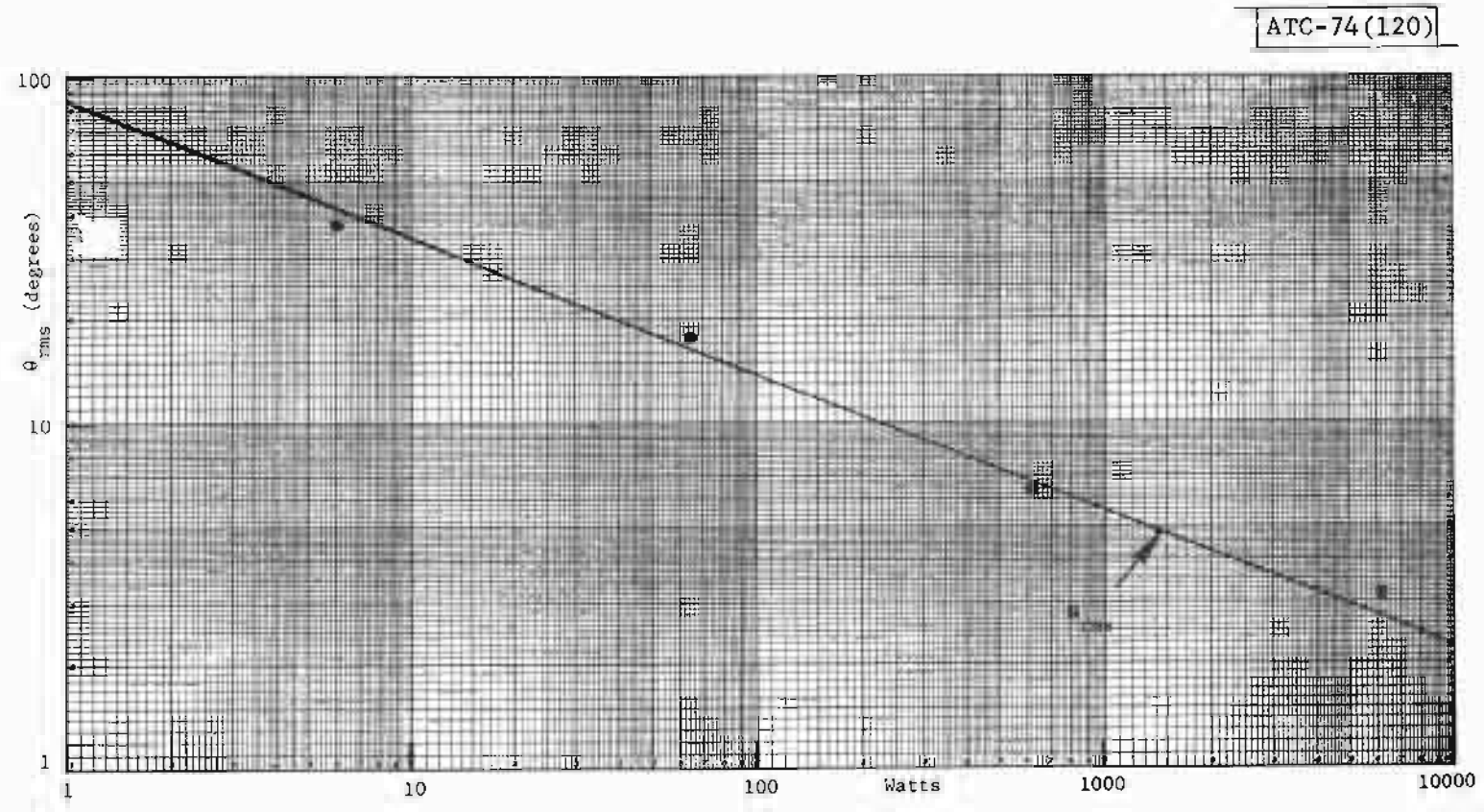

Fig. 120. Phase error (rms) vs priming power.

It appears that it would require an excessive amount of priming (in the order of the magnetron output power itself) in order to develop a reasonable ϕ of -40 dB.

G. OTP Compliance

The Office of Telecommunications Policy (OTP) radar design objectives are inappropriate in the context of the present study. The OTP design objectives* relate the allowed spectral bandwidth to the rise time of the RF envelope; the longer the rise time the narrower the bandwidth. There is little one can do to control the rise time of a magnetron, coaxial or standard. Because coaxial tubes have a longer rise time, the OTP objectives require that the coaxial tube operate in narrower bandwidth. Figures 121 and 122 illustrate this point. Figure 121 is the coaxial magnetron spectrum with the OTP specs overlaid, while Figure 122 is the standard tube. Notice that the standard tube is allowed twice the bandwidth of the coaxial tube. In spite of this restriction, the coaxial tube is within OTP specs while the DX276 is not.

IV. CONCLUSIONS

Measurements have been made of a coaxial magnetron, the Raytheon QK1739LL, and a conventional magnetron, the Amperex DX276, in order to compare their performance. Each has advantages over the other. Whether one is better overall than the other depends on the situation. Some of the disadvantages can be corrected by the radar design. The following is a list of comparative magnetron properties, and following it is an assessment of whether they are significant. The plus (+) indicates superiority.

	Coaxial	Standard
Pulling	+	
Pushing	+	
Frequency Jitter		+
Time Jitter		+
Spurious Spectrum	+	
Long-term Stability	+	
Lifetime	+	
Break-in Time	+	
Cost		+

*OTP Manual of Regulations and Procedures for Radio Frequency Management, Chapter 5, Section 5.3 (January 1973).

ATC-74(121)

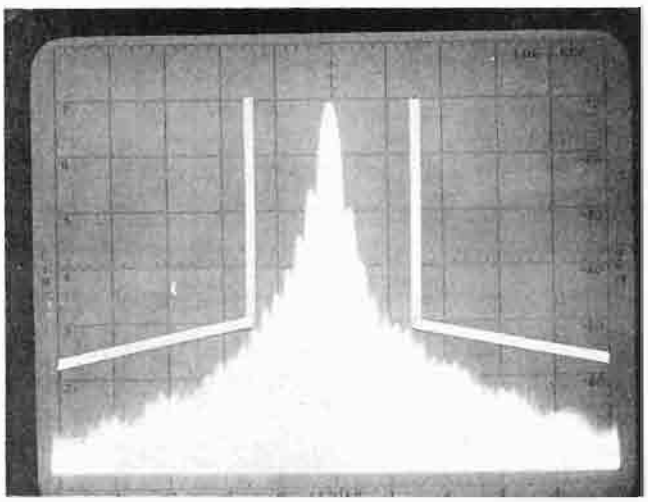

Fig. 121. OTP specification superimposed on coaxial magnetron (V-axis: 10 dB/div; H-axis: 5 MHz/div).

ATC-74(122)

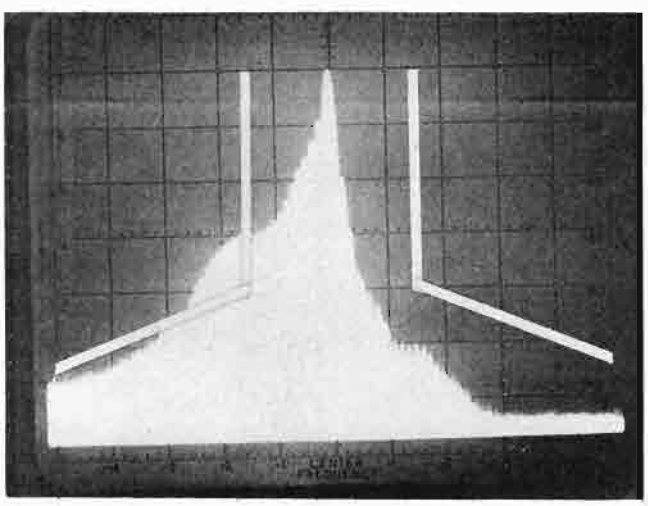

Fig. 122. OTP specification superimposed on DX-276 (V-axis: 10 dB/div; H-axis: 10 MHz/div).

Pulling; can be alleviated by the use of an isolator or circulator. The ASR-7 uses a circulator; therefore, it is not a problem for either tube.

Pushing: can be reduced by good modulator design. The ASR-7 is probably adequate for either tube.

Frequency Jitter: is intrinsic and is not affected by modulator design.

Time Jitter; is intrinsic and the most serious problem of coaxial tubes. It can be partially corrected by priming and rise time control. The ASR's already have a circulator that can be used to inject the priming signal.

The Near-in Spurious Spectrum of either tube cannot be improved, however harmonics and high frequencies could be removed with waveguide filters.

Long-Term Stability can be corrected by AFC-ing the magnetron with respect to a crystal-controlled local oscillator. The crystal oscillator has the stability needed for a high performance MTI or MTD system.

The Lifetime and reliability of coaxial magnetrons is expected to be much greater than that of the standard magnetron because of its larger internal structure. This structure permits lower electric fields, essentially eliminating sparking and Break-in Time.

The coaxial tube Costs about a factor of 10 more than the standard tube. The cost may be reduced by mass production and/or a competitive market.

APPENDIX

EFFECT OF PULSE-TO-PULSE FM ON THE PERFORMANCE OF A COHERENT RADAR PROCESSOR SUCH AS THE LINCOLN LABORATORY MOVING TARGET DETECTOR (MTD)

INTRODUCTION

The frequency instability of a magnetron in a radar manifests itself as a modulation of the return from an interval of clutter. This modulation can be either periodic or random. The periodic modulation is caused, for example, by external perturbations of the magnetron via the high voltage power supply, the heater supply or external AC magnetic fields. These effects can be removed by careful modulator and power supply designs. However, there is an intrinsic random modulation that exists in all magnetrons and different magnetrons have differing stabilities. It is the effect of this random noise modulation on the radar performance that is treated here.

THEORY

Consider an extent of radar clutter return, C(t). For our purposes the clutter return is frozen and the antenna is not rotating. The clutter does not vary from one pulse interperiod to the next. That is:

$$C(t) = C\left(t - \frac{1}{(prf)}\right) \qquad (1)$$

where: (prf) is the pulse repetition frequency. C(t) is considered to be fine structured compared to the magnetron pulse length and of the order of a half wave length of the radar frequency. Thus, C(t) has a resolution of about 5 cm for an S-band radar. If we let the magnetron RF pulse envelope be represented by u(t) and the phase deviation of the magnetron from its norm by $\theta(t)$, then the return from a stationary point reflector becomes

$$u(t) = e^{i\tilde{\theta}(t)}$$

The squiggle above $\tilde{\theta}(t)$ is to remind one that $\tilde{\theta}(t)$ is a random variable (rv). The signal returning to the radar is then

$$\tilde{S}(t) = \tilde{C}(t) \otimes u(t)\ e^{i\tilde{\theta}(t)} \tag{2}$$

where $\otimes$ represents the convolution operator. $\tilde{C}(t)$ fluctuates only during an interpulse period, while $\tilde{\theta}(t)$ can fluctuate between periods. The average value of $\tilde{S}(t)$ at the time t is then

$$\bar{\tilde{S}}(t) = \bar{\tilde{C}}(t) \otimes u(t) \tag{3}$$

Notice that $\bar{\tilde{S}}(t)$ is still a random variable but only during the interpulse period. Most radar processors (MTD, MTI cancellers) remove $\bar{\tilde{S}}(t)$, consequently the residue $\tilde{S}(t) - \bar{\tilde{S}}(t)$ is of prime importance. The variance of S(t) is the average power remaining after the mean has been removed. The variance is given by

$$\sigma^2 = E\left\{\left[\left(\tilde{S}(t) - \bar{\tilde{S}}(t)\right)\ \left(\tilde{S}(t) - \bar{\tilde{S}}(t)\right]^*\right\} \tag{4}$$

where E{ } is the expectation operator (or average) and the asterisk represents the complex conjugate. Thus, the quantity

$$\phi \triangleq \frac{\sigma^2}{E\{\tilde{S}^2\}}$$

is the residue-to-clutter ratio and is a measure of the magnetron stability. Applying (2) and (3) we have

$$\sigma^2 = E\left\{\left[\tilde{C}(t) \otimes u(t)\ (e^{i\tilde{\theta}(t)} - 1)\right]\left[\tilde{C}^*(t) \otimes u(t)\ (e^{-i\tilde{\theta}(t)} - 1)\right]\right\} \tag{5}$$

Because $\tilde{\theta}(t)$ is of the order of a few degrees, the following approximation is made.

$$\sigma^2 = E\ \left\{\left[\tilde{C}(t) \otimes u(t)\ i\tilde{\theta}\ (t)\right]\left[\tilde{C}^*(t) \otimes u(t)\ (-i)\ \tilde{\theta}(t)\right]\right\} \tag{6}$$

The magnetron envelope is assumed to extend from T_o to $T_o + T$ and to have a rectangular shape. Thus, from the definition of convolution we have

$$\sigma^2 = E\left\{ \int_{T_o}^{T_o+T} \hat{C}(t-\tau)\ \hat{\theta}(t)\ dt \int_{T_o}^{T_o+T} \hat{C}^*(t'-\tau)\ \hat{\theta}(t')\ dt' \right\} \quad (7)$$

or

$$\sigma^2 = E\left\{ \int_{T_o}^{T_o+T} \int_{T_o}^{T_o+T} \hat{C}(t'-\tau)\ \hat{C}^*(t-\tau)\ \hat{\theta}(t)\ \theta(t')\ dt\ dt' \right\} \quad (8)$$

Since $\hat{C}(t-\tau)\ \hat{C}^*(t'-\tau)$ and $\hat{\theta}(t)\ \hat{\theta}(t')$ are independent random variables, we can apply the expectation operator separately,

$$\sigma^2 = \int_{T_o}^{T_o+T} \int_{T_o}^{T_o+T} R_c(t-t')\ E\left\{\hat{\theta}(t)\ \hat{\theta}(t')\right\}\ dt\ dt' \quad (9)$$

where

$$R_c(t-t') = E\left\{\hat{C}(t-\tau)\ \hat{C}^*(t'-\tau)\right\}$$

is approximately an impulse shaped covariance function. Thus, we can evaluate the inner integral and find

$$\sigma^2 = \int_{T_o}^{T_o+T} C_o\ E\left\{\hat{\theta}^2(t')\right\}\ dt' \quad (10)$$

where: C_o is the area under the impulse function R_c. That is

$$C_o \triangleq \int_{-\infty}^{\infty} R_c(t)\ dt$$

The function $\tilde{\theta}(t)$ is not known, however it cannot be a constant otherwise no FM could take place. The simplest time dependence would be of the linear form

$$\tilde{\theta}(t) = \tilde{\omega} t \tag{11}$$

Any higher order dependence cannot be measured with our present equipment and it is not clear that it exists. $\tilde{\omega}$ is a random variable representing the random frequency error of the magnetron. Taking (11) as our model we find

$$\sigma^2 = C_o \, E\left\{\tilde{\omega}^2\right\} \int_{T_o}^{T_o+T} t^2 \, dt$$

$$= E\left\{\tilde{\omega}^2\right\} \frac{C_o}{3} \left[(T_o + T)^3 - T_o^3\right] \tag{12}$$

In a similar manner we find

$$E\left\{\tilde{\tilde{S}}^2(t)\right\} = \int_{T_o}^{T_o+T} \int_{T_o}^{T_o+T} R_c(t-t') \, dt \, dt' = C_o T \tag{13}$$

Thus the residue-to-clutter ratio is:

$$\phi \triangleq \frac{\sigma^2}{E\left\{\tilde{\tilde{S}}^2\right\}} = E\left\{\tilde{\omega}^2\right\} \frac{(T_o + T)^3 - T_o}{3T} \tag{14}$$

The lowest residue occurs when $T_o = T/2$, then:

$$\phi = E\left\{\tilde{\omega}^2\right\} \frac{T^2}{12} \tag{15}$$

This corresponds to locking the coho to the center of the magnetron pulse. If the coho is locked to the tail-end of the magnetron pulse, $T_o = -T$, then:

$$\phi = E\left\{\tilde{\omega}^2\right\} \frac{T^2}{3} \tag{16}$$

EXAMPLE OF THE RAYTHEON QK1739 COAXIAL MAGNETRON IN THE ASR-7

If we assume a residue-to-clutter ratio ϕ of 0.16×10^{-4} and a pulse length of 0.7 microseconds, then for a center-locking system

$$f_{rms} \triangleq \frac{1}{2\pi} \sqrt{E\{\omega^2\}} = \frac{1}{2\pi} \sqrt{\frac{12\phi}{T^2}}$$

$$= \frac{2}{\pi T} \sqrt{3\phi} = 3150 \text{ Hz}$$

In the magnetron stability tester the output is given by

$$\theta_{rms} = 2\pi \, f_{rms} \, T_d \, \sqrt{6}$$

where T_d is the delay line delay of 0.35 microseconds and $\sqrt{6}$ is the gain of the three-pulse canceller to a white random signal. Thus, the output (in degrees) is:

$$\theta_{rms} \leq 360 \, f_{rms} \, T_d \, \sqrt{6} = 0.97 \text{ degrees}$$

If tail-end locking is used, then 0.49 degrees is required. The value of $\phi = 0.16 \times 10^{-4}$ was chosen to limit the loss in processor improvement factor to 0.64 dB when operating at a clutter-to-thermal noise ratio (C/N) of 40 dB.

$$10 \log \left(\frac{N/C + .16 \, N/C}{N/C}\right) = 0.64 \text{ dB}$$

If we were to allow the residue ϕ to be equal to the thermal noise N, the improvement ratio would deteriorate by 3 dB. ϕ would be equal to 10^{-4} and the output of the stability tester would be

$$\theta_{rms} = 360 \, T_d \, \sqrt{6} \, \frac{2}{\pi T} \, \sqrt{3\phi} = 2.43^{\circ} \qquad (18)$$

This happens to be equal to the value measured for the coaxial magnetron at 2700 MHz at its nominal heater power. At higher heater power (which may reduce tube life) θ_{rms} can drop to 0.5 degrees.

CONCLUSION

A model has been proposed to calculate the effect of pulse-to-pulse FM of magnetrons in the presence of clutter on the performance of a coherent processor. It establishes a simple relation between frequency stability and clutter rejection useful in predicting the performance of magnetron radars.

ACKNOWLEDGEMENT

Acknowledgement is given to Mr. Harry P. McCabe, Engineering Assistant. Mr. McCabe set up the equipment, performed virtually all the measurements and provided many useful suggestions.